Supplementary Information

Real-time observation of a metal complex-driven reaction intermediate using a porous protein crystal and serial femtosecond crystallography

Basudev Maity,[1*] Mitsuo Shoji,[2*] Fangjia Luo,[3] Takanori Nakane,[4] Satoshi Abe,[1] Shigeki Owada[3,5] Jungmin Kang,[5] Kensuke Tono,[3,5] Rie Tanaka,[5,6] Thuc Toan Pham,[1] Mariko Kojima,[1] Yuki Hishikawa,[1] Junko Tanaka,[1] Jiaxin Tian,[1] Misaki Nagama,[1] Taiga Suzuki,[1] Hiroki Noya,[1] Yuto Nakasuji,[1] Asuka Asanuma,[1] Xinchen Yao,[1] So Iwata,[5,6] Yasuteru Shigeta,[2] Eriko Nango,[5,7*] Takafumi Ueno.[1,8*]

[1] *School of Life Science and Technology, Tokyo Institute of Technology, Nagatsuta-cho 4259, Midori-ku, Yokohama, Japan.*

[2] *Center for Computational Sciences, University of Tsukuba, 1-1-1 Tennodai, Tsukuba, Ibaraki 305-8577, Japan.*

[3] *JASRI, 1-1-1, Kouto, Sayo-cho, Sayo-gun, Hyogo 679-5198 Japan*

[4] *Institute of protein research, Osaka University.*

[5] *RIKEN SPring-8 Center, Hyogo 679-5148, Japan*

[6] *Department of Cell Biology, Graduate School of Medicine, Kyoto University.*

[7] *Tohoku University. Institute of Multidisciplinary Research for Advanced Materials, Tohoku University*

[8] *Research Center for Autonomous Systems Materialogy (ASMat) Institute of Innovative Research, Tokyo Institute of Technology, Nagatsuta-cho 4259, Midori-ku, Yokohama, Japan*

Supplementary Methods

Structure refinement

All the structure refinements were done with the Phenix suite.[1] The protein models were located by Phaser[2] using the PDB entry 193L[3] as a starting model. The model building was done in COOT followed by refinement in phenix.refine. The processes were continued until a reasonable model was built. Water molecules were modelled automatically in COOT with a cutoff difference density map at 3.0 σ and weak density waters were modelled manually. Highly coordinated water molecules at Asp35 and Asp101 in some structures were tentatively assigned as Na^+ ions. Sidechains of the residues Gln121, Arg125 and Arg128 in some structures were truncated due to lack of sufficient density.

The presence of $[Mn(CO)_3(wat)_2]^+$ moiety in the structure under darkness was identified by comparing with a metal-free HEWL structure. To confirm this, we performed a similar reaction using a single crystal which gave a similar density map, and the Mn ion was confirmed by anomalous density at 6σ (Supplementary Figure 1). This is consistent with the previous report on HEWL-$Mn(CO)_3$ structure.[4] The assignment of $Mn(CO)_3(wat)_2$ moiety was further validated by omit map (phase bias) and Polder map (bulk solvent contribution). The structures of $Mn(CO)_3(wat)_2$ after light irradiation was modelled based on the combination of $2F_o$-F_c maps (F_o and F_c are the observed and calculated structure factor amplitude) and isomorphous difference maps with dark structures. During the initial stages of refinement, both B-factor (displacement of the atomic position from an average (mean) value(mean-square displacement)) and occupancy were allowed to refine freely. In the later stages of model building, the occupancy values at Mn center were adjusted to keep the B-factor of Mn ion close to the coordinating atom (N^{ε}) of His15. The resulting Mn coordination structures were validated using the check my metal server (https://cmm.minorlab.org/).

Difference maps (F_o-F_o) were calculated by the "Isomorphous difference map" task in the Phenix GUI. A complete darkness data was collected each beam time and used as a phase and amplitude reference. It is to be noted that since the interleaved dark data were collected in between two light data sets (see the setting in Fig-4b), there is a possibility of light contamination in interleaved dark data. Therefore, we always considered the difference maps obtained against the complete darkness data in which no laser was used. To evaluate the light contamination, difference maps against interleaved dark were calculated as shown in Supplementary Figure 6a in SI. In addition, we also performed the experiment with negative delay in which light was irradiated after XFEL pulse (Supplementary Figure 6b,c).

For quantification, difference density maxima were measured in COOT in units of e/Å3 as well as σ (root mean square electron density of the unit cell) in Supplementary Table 6 but were assigned as zero if features were not identifiably as distinct peak.[5] Similarly, the omit map densities were also

measured to estimate the apparent occupancy of the released CO or Mn. The data are plotted and shown in Supplementary Figure 9.

All the structures were validated in Molprobity[6] and deposited in wwPDB server with accession code (8WZF, 8WZG, 8WZR, 8WZT and 8WZV).

Validity of the QM/MM theoretical level

Dependences of the theoretical condition such as basis set, DFT functional and QM region to the peak top of the absorption spectra and the first excited energy are shown in Supplementary Table 7. RMSD values of the Mn center by using larger basis sets are 0.228Å(DZVP), 0.216Å(TZVP), and 0.216 Å(TZVP+) compared to the X-ray structure (Supplementary Figure 13). This result means that the geometrical structures are only improved by 0.008 Å, even for the larger basis set. On the other hand, the excited state property, such as peak-top wave number around 400 nm, is very sensitive to the basis sets (384(entry 2) – 387(entry 1) = –3 nm), DFT functional (389 (entry 6) – 386 (entry 3) = +3 nm) and QM region (394(entry 9)- 389(enety6) = 5 nm). Even though the optimized geometry by using TZVP(B2) does not improve for the peak-top wavelength compared to the structures calculated by using DZVP (394(entry12)-394(entry9) = 0 nm), considering the computational costs, large number of structural optimizations should be performed at the B3LYP/DZVP(B1) theoretical level, while the few UV spectra calculations can be carried out at the larger basis set and larger QM region as the same level of entry 9 in Supplementary Table 7.

Comparison between QM/MM optimized structures and TR-SFX structures

Direct comparisons of the bond distances around the Mn center and root-mean-square deviation (RMSD) among the QM/MM optimized structures and the SFX results are shown in Supplementary Table 5 and 6. The average Mn-C coordination length of the QM/MM optimized structure **1** is 1.81 Å, slightly shorter compared to the corresponding one of 1.94 Å in SFX result (PDBID:8WZF). The average Mn-O coordination length in QM/MM structure **1** is 2.12Å corresponding to the SFX (PDBID:8WZF) result of 2.24 Å. In both cases, the difference between QM/MM and SFX results is about -0.12 Å, and this trend is very similar in other states. From the RMSD values around the Mn center (Supplementary Table 6), the closest SFX structures from QM/MM structures (**1**-**3**) are commonly complete dark SFX model (**8WZF**), whereas the closest QM/MM structures from SFX structures become **1**, **2** and **3** for SFX structures of (**8WZF**) complete dark, (**8WZG**) 10ns 20μJ (**8WZV**) 1μs 40μJ, respectively. Larger RMSD values of around 0.2 Å come from the larger disorder at the equatorial water ligands, not CO ligands. This implies the flexibility of the water coordination. The RMSD results indicate that structural similarity is highest in the initial non-photoexcited state, and the structural similarity becomes relatively worse as the reaction proceeds after the

photoexcitation. It should be emphasized that the closest QM/MM structure in actual species corresponds best to the SFX structure. Based on these detailed structural comparisons, SFX structures reflect the photochemical reaction.

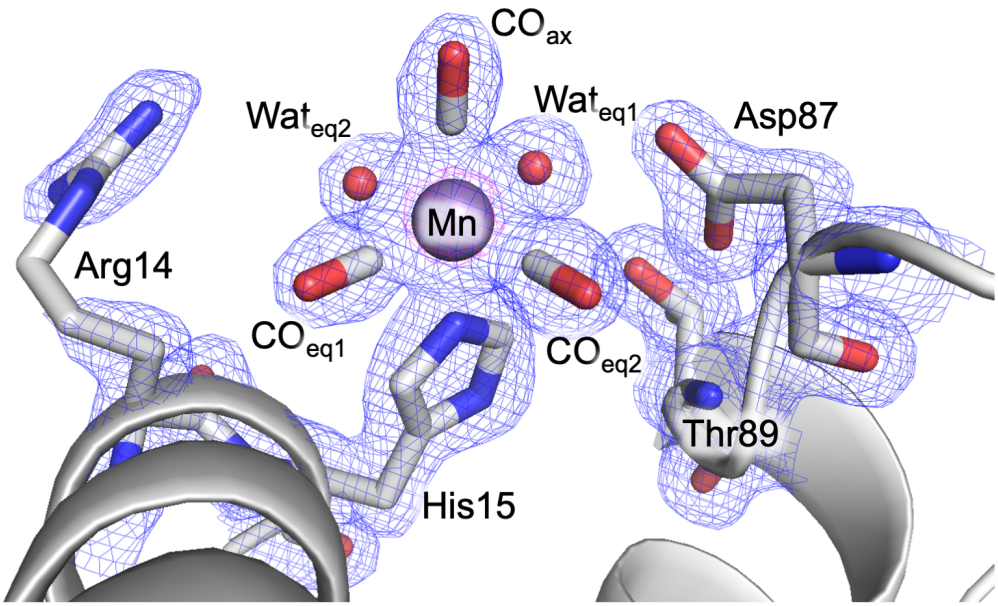

Supplementary Figure 1: The structure of HEWL-Mn(CO)$_3$(wat)$_2$ determined from a single crystal at 100K. The $2F_o$-F_c map at 1σ and anomalous map at 6σ are shown in blue and magenta mesh, respectively.

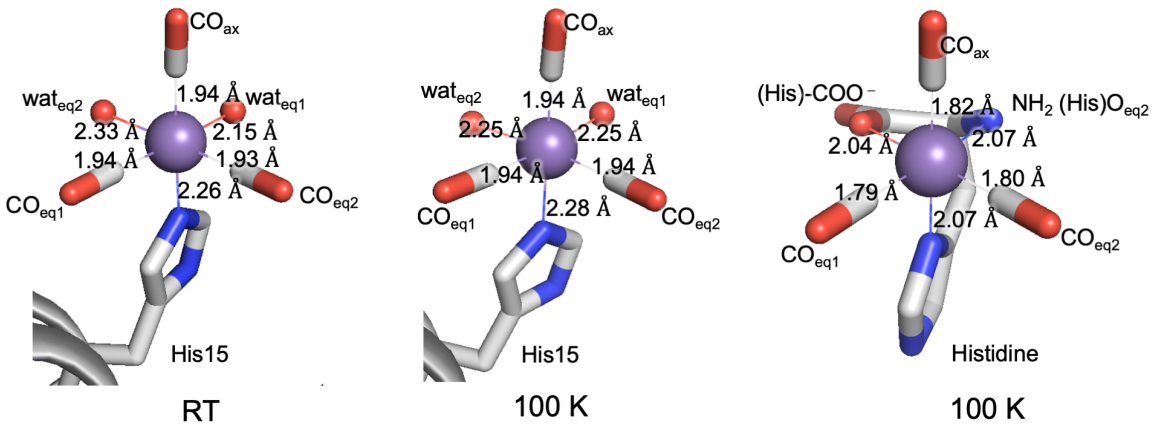

Supplementary Figure 2: Comparison of the coordination structure of Mn(CO)$_3$(wat)$_2$ moiety in (a) HEWL-Mn(CO)$_3$(wat)$_2$ at RT (b) HEWL-Mn(CO)$_3$(wat)$_2$ at 100 K and (c) Histidine-Mn(CO)$_3$ at 100 K. Color codes are as follows: Carbon: grey; Nitrogen: blue; Oxygen: red; Manganese: purple. Microcrystals were used for RT data collection by serial crystallography.

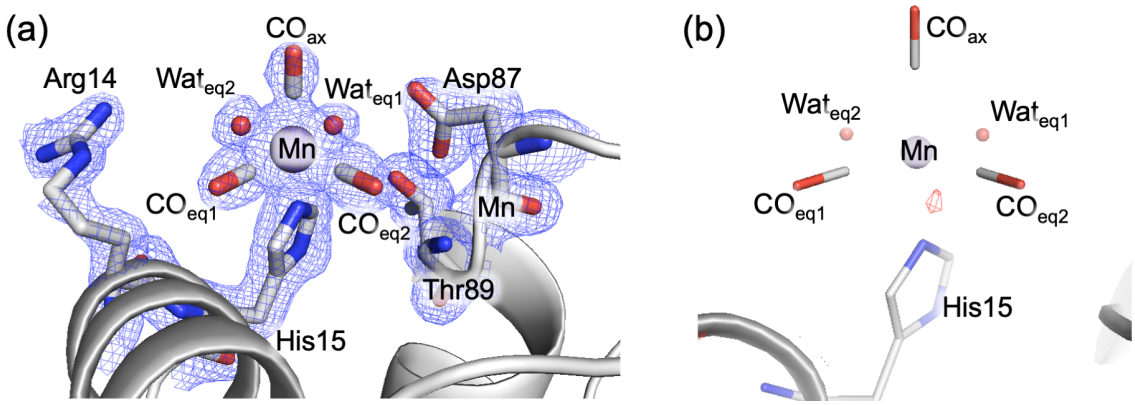

Supplementary Figure 3: (a) The structure of HEWL-Mn(CO)$_3$(wat)$_2$ under darkness. The structure was collected with an interval of 24h time to see the possibility of any dark reaction in comparison to the darkness structure shown in the Figure 3b in main text. The $2F_o$-F_c map contoured at 1σ is shown blue mesh. (b) The F_{data2}-F_{data1} map (F_o-F_o) contoured at ±3.2 σ is shown in green (positive) and red (negative). The data were collected under dark conditions at RT by SFX.

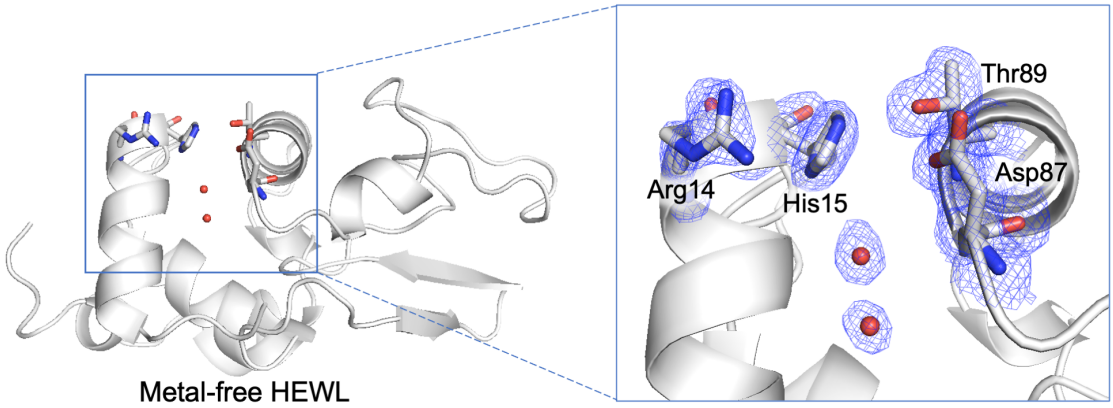

Supplementary Figure 4: Crystal structure of a metal-free HEWL structure as determined by SFX. The metal binding site at His15 and the surrounding Arg14, Asp87 and Thr89 residues are highlighted by stick model. The $2F_o$-F_c electron density map surrounding the Arg14, His15, Asp87 and Thr89 are shown in blue mesh contoured at 1.0 σ.

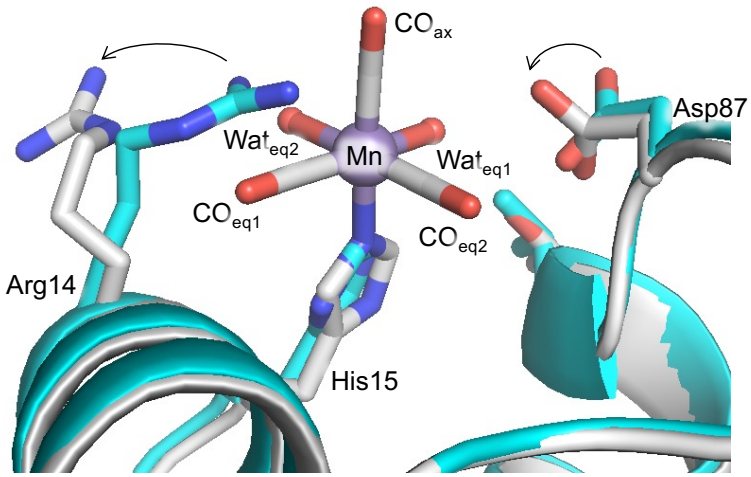

Supplementary Figure 5: Structural overlap of the metal-free HEWL (cyan) and HEWL-$Mn(CO)_3(wat)_2$ (grey) structures showing the conformational changes of Arg14 and Asp87 after metal binding. Color code for metal-free HEWL: Cartoon, cyan; carbon, cyan; nitrogen, blue; oxygen, red. Color code for HEWL-$Mn(CO)_3(wat)_2$: Cartoon, grey; carbon, grey; nitrogen, blue; oxygen, red; Manganese, purple.

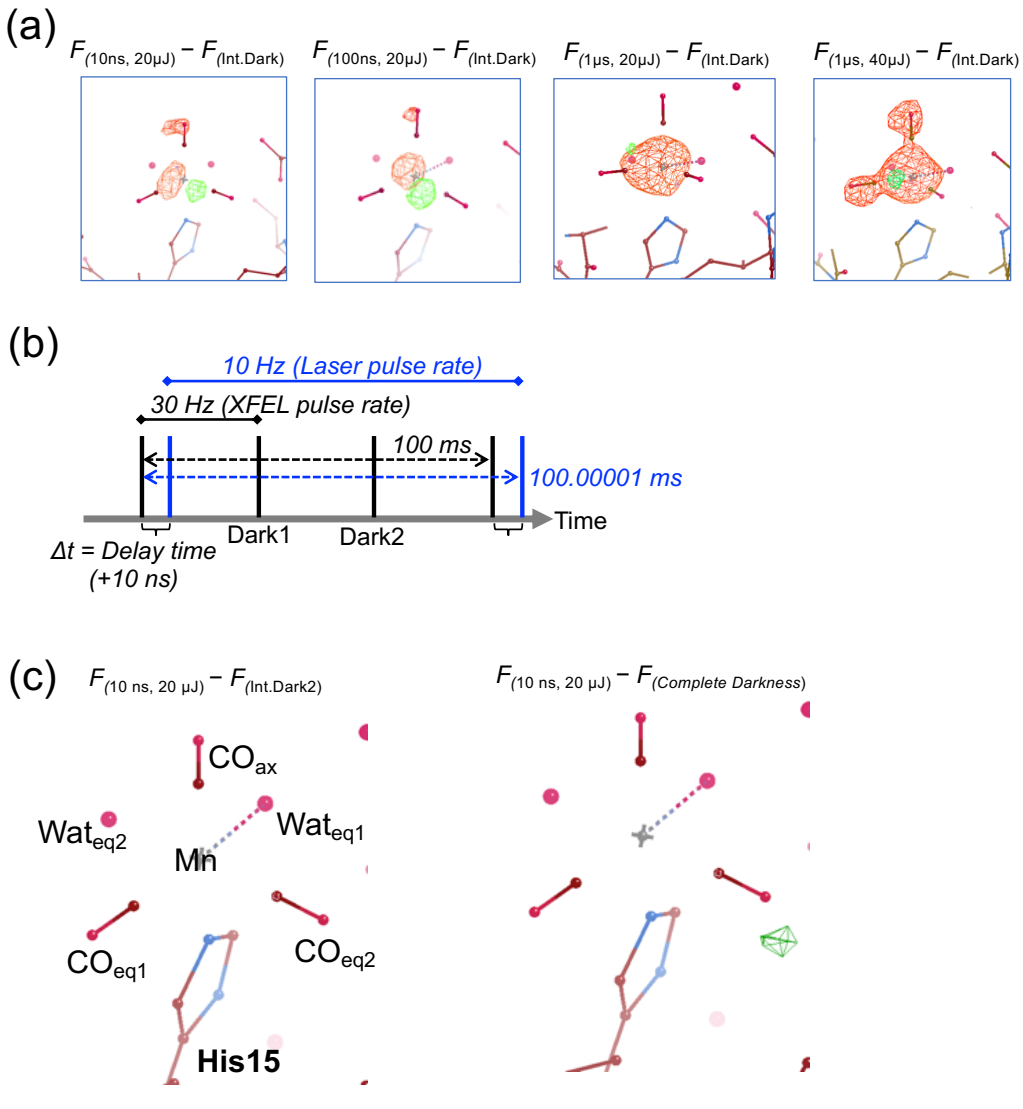

Supplementary Figure 6: (a) The difference F_{light}-F_{dark} map (at ±3.0σ, green/red) with respect to the respective interleaved dark structure showing the ligand release during the reaction. (b) A typical setup for the measurement by fixing negative delay (+10 ns) in which light is irradiated after X-ray diffraction to check any possibility of light contamination. (c) The difference density features (at 3.0 σ) on Mn-carbonyl in the negative delay experiment. No difference density feature indicates no light contamination.

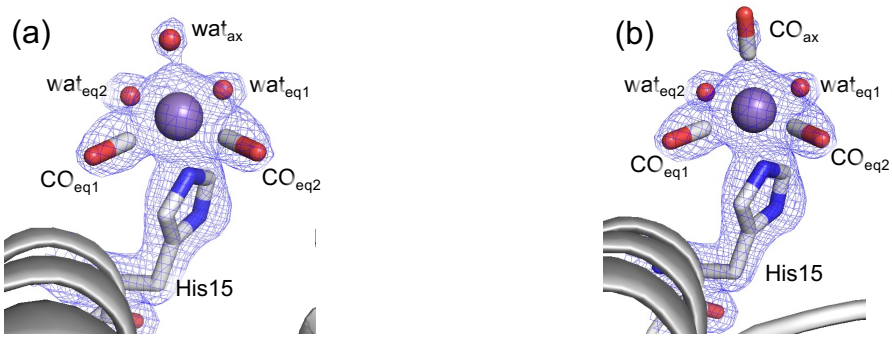

Model: HEWL-Mn(CO)$_2$(wat)$_3$

atom	occupancy	B-factor
Mn	0.9	31.12
His15, NE2	1	31.53
wat$_{ax}$, O	0.9	35.12
CO$_{eq1}$, C	0.9	29.98
CO$_{eq1}$, O	0.9	36.60
CO$_{eq2}$, C	0.9	31.70
CO$_{eq2}$, O	0.9	34.23
Wat$_{eq1}$,O	0.9	33.83
Wat$_{eq2}$,O	0.9	39.51
R-work (R-free)	18.57 (20.07)	

Model: HEWL-Mn(CO)$_3$(wat)$_2$

atom	occupancy	B-factor
Mn	0.9	31.45
His15, NE2	1	31.05
CO$_{ax}$, C	0.9	37.41
CO$_{ax}$, O	0.9	45.10
CO$_{eq1}$, C	0.9	30.65
CO$_{eq1}$, O	0.9	37.26
CO$_{eq2}$, C	0.9	32.52
CO$_{eq2}$, O	0.9	34.73
Wat$_{eq1}$,O	0.9	33.48
Wat$_{eq2}$,O	0.9	39.85
R-work (R-free)	18.50 (20.03)	

Supplementary Figure 7: Assignment of the axial ligand in the HEWL-Mn(CO)$_3$(wat)$_2$ structure, 10 ns after the photoexcitation (Laser intensity 20 uJ). (a) Occupancy and B-factors (Å^2) of selected atoms when the axial ligand is assigned to a water molecule. (b) Occupancy and B-factors (Å^2) when the axial ligand is assigned to CO ligand. The $2F_o$-F_c maps in both images are contoured at 1.2σ and shown as blue mesh. The high B-factor and spherical $2F_o$-F_c map density of the axial ligand in (b) suggest that the assignment of a water molecule for the axial ligand in (a) might be more accurate.

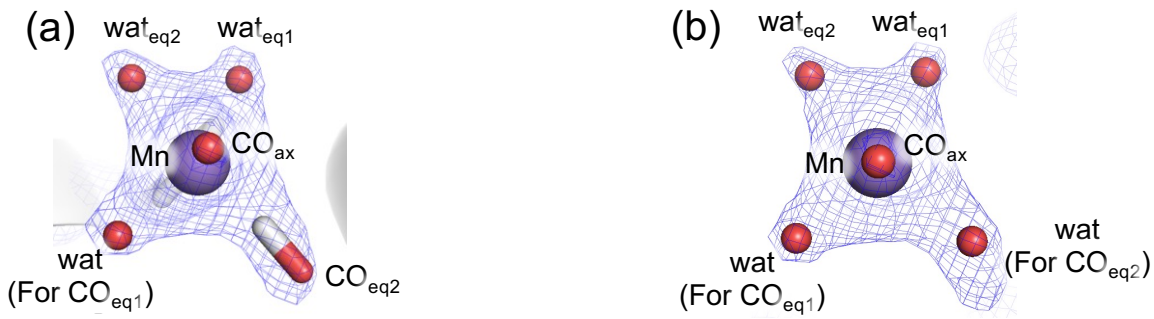

Model: HEWL-Mn(CO)(wat)$_4$			**Model:** HEWL-Mn(wat)$_5$		
atom	**occupancy**	**B-factor**	**atom**	**occupancy**	**B-factor**
Mn	0.65	44.14	**Mn**	0.65	43.9
His15, NE2	1.0	45.60	**His15, NE2**	1.0	44.3
Wat$_{ax}$	0.65	46.85	**Wat$_{ax}$**	0.65	44.7
Wat (for CO$_{eq1}$)	0.65	45.53	**Wat (for CO$_{eq1}$)**	0.65	44.6
CO$_{eq2}$, C	0.65	40.91	**Wat (for CO$_{eq2}$)**	0.65	41.4
CO$_{eq2}$, O	0.65	44.45			
Wat$_{eq1}$, O	0.65	48.50	**Wat$_{eq1}$, O**	0.65	45.9
Wat$_{eq2}$, O	0.65	52.09	**Wat$_{eq2}$, O**	0.65	49.7
R-work (R$_{free}$)	0.1902 (0.1913)		**R-work (R$_{free}$)**	0.1903 (0.1987)	

Supplementary Figure 8: Assignment of the equatorial (eq2) ligand in the HEWL-Mn(CO)$_3$(wat)$_2$ structure, 1μs after the photoexcitation (Laser intensity 40 uJ). (a) Occupancy and B-factors (Å^2) of selected atoms when the eq2 ligand is assigned to a CO ligand. (b) Occupancy and B-factors (Å^2) when the eq2 ligand is assigned to a water. The $2F_o$-F_c map contoured at 1σ is shown in blue mesh in both figures (view from CO_{ax}). Considering the $2F_o$-F_c , F_o-F_c and omit map shape at eq2 position, assignment of a CO ligand might be more accurate than a water.

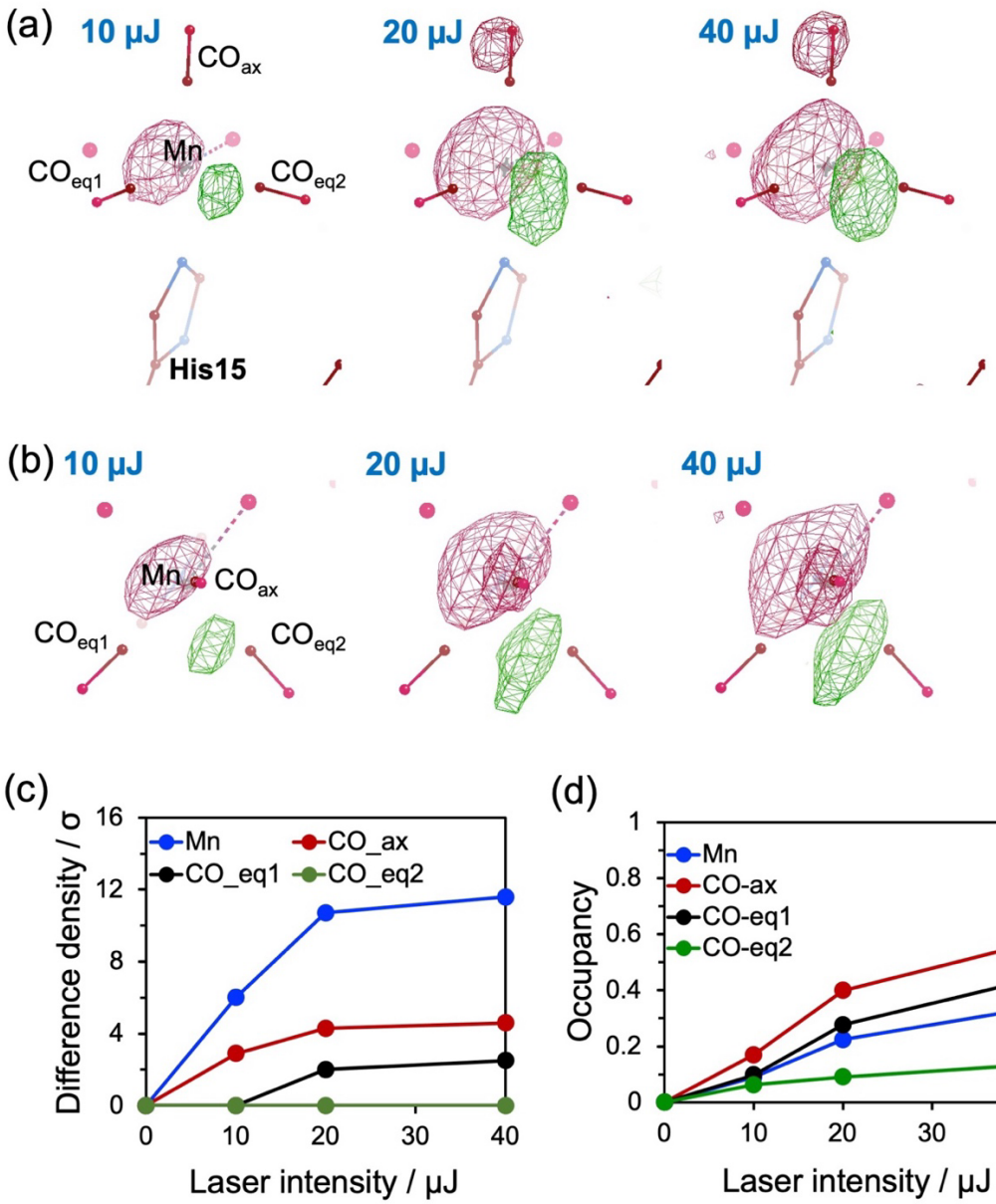

Supplementary Figure 9A: Power titration of the CO release reaction in HEWL-$Mn(CO)_3$ for 10 ns delay. The data presented are from an independent experiment measured at the same beamtime. (a) The difference $|F_{obs}|^{light}$ -$|F_{obs}|^{comp.dark}$ map (at ±3.2σ, green/red) with respect to the structure under darkness showing the ligand release during the reaction at laser intensity 10 µJ, 20 µJ and 40 µJ. The maps are shown on the model under complete darkness. (b) View of the difference $|F_{obs}|^{light}$ -$|F_{obs}|^{comp.dark}$ map from the direction of CO_{ax} corresponding to the images as shown in (a). (c) Plot of difference density feature (negative) vs laser intensity to show the effect of laser intensity on CO release reaction. The density feature ($|F_{obs}|^{light}$ -$|F_{obs}|^{comp.dark}$) below 2.0σ are considered insignificant due to high signal to noise ratio. (d) Plot showing the apparent occupancy vs laser intensity. The apparent occupancy of the released CO or Mn was calculated based on the respective omit map density in dark and light irradiated state using the formula: Occupancy = (dark state-light state)/dark state.

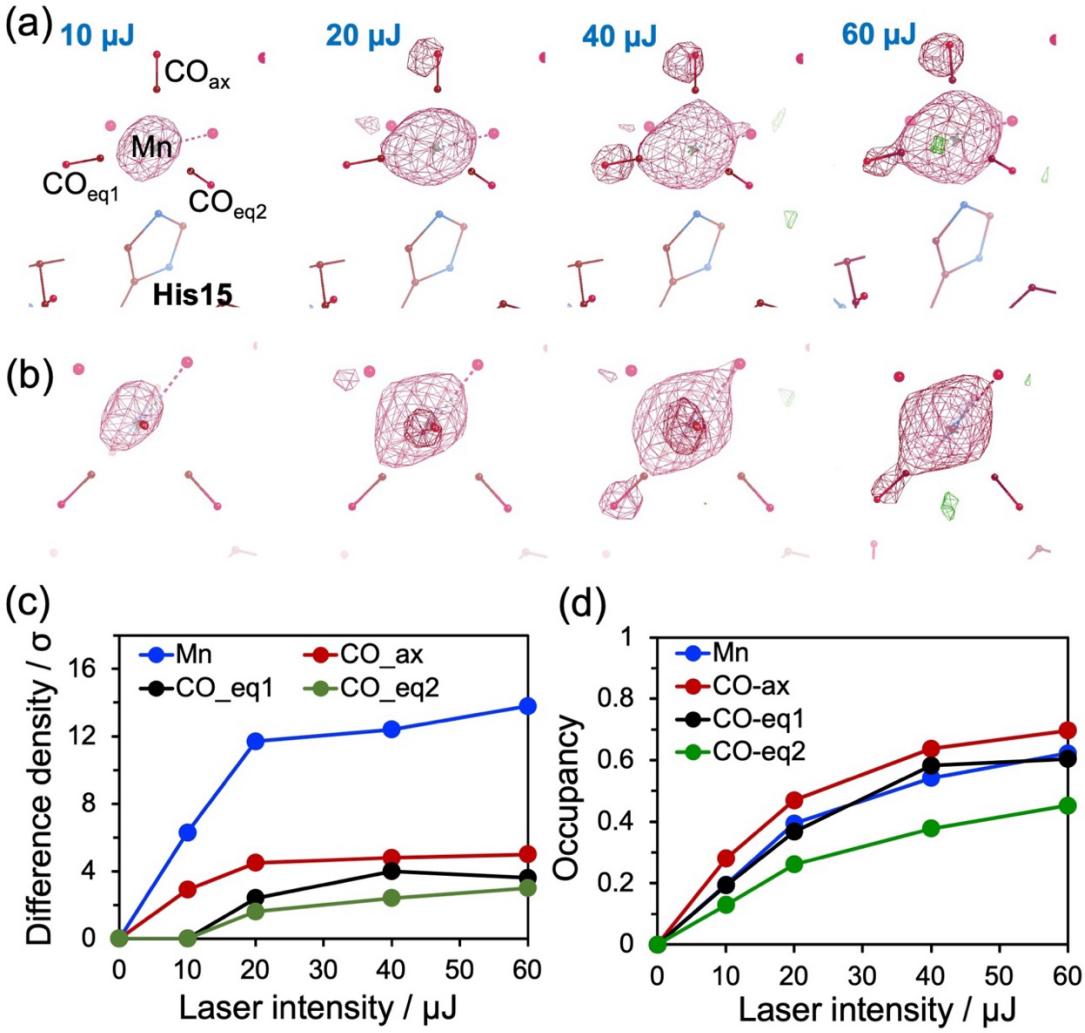

Supplementary Figure 9B: Power titration of the CO release reaction in HEWL-$Mn(CO)_3$ for 1 µs delay. The data presented are from an independent experiment measured at the same beamtime. (a) The difference $|F_{obs}|^{light}$ -$|F_{obs}|^{comp.dark}$ map (at ±3.2σ, green/red) with respect to structure under darkness showing the ligand release during the reaction at laser intensity 10 µJ, 20 µJ and 40 µJ. The maps are shown on the model under complete darkness. (b) View of the difference $|F_{obs}|^{light}$ - $|F_{obs}|^{comp.dark}$ map from the direction of CO_{ax} corresponding to the images as shown in (a). (c) Plot of difference density feature (negative) vs laser intensity to show the effect of laser intensity on CO release reaction. The density feature ($|F_{obs}|^{light}$ -$|F_{obs}|^{comp.dark}$) below 2.0σ are considered insignificant due to high signal to noise ratio. (d) Plot showing the apparent occupancy vs laser intensity. The apparent occupancy of the released CO or Mn was calculated based on the respective omit map density in dark and light irradiated state using the formula: Occupancy = (dark state-light state)/dark state.

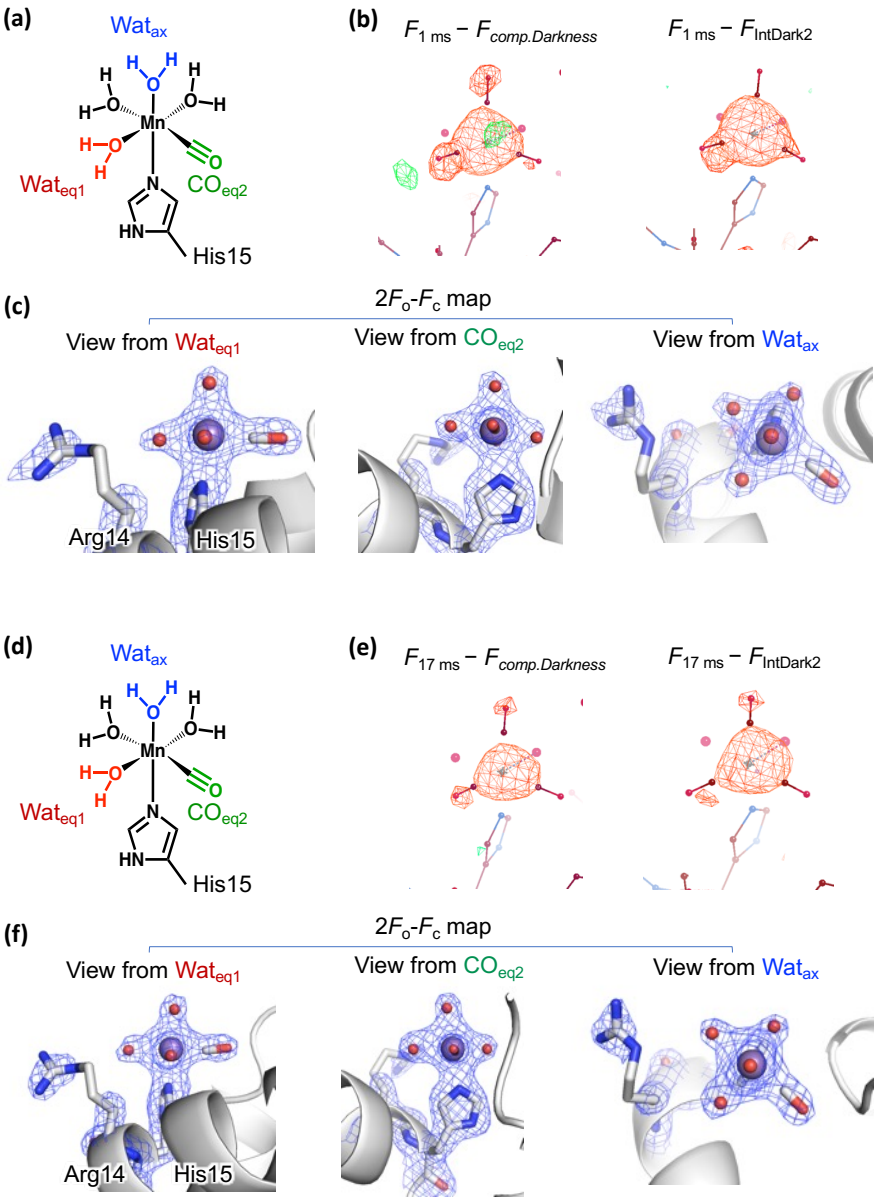

Supplementary Figure 10: Analysis of HEWL-Mn(CO)$_3$(wat)$_2$ structure at longer delay after the photoexcitation. (a) Coordination structure of HEWL-Mn(CO)$_3$(wat)$_2$ after 1ms of photoexcitation with 20 μJ laser intensity. (b) The difference F_{light}-F_{dark} map (at ±3.0σ, green/red) against complete dark and the difference F_{light}-F_{dark} map (at ±3.0σ, green/red) against interleaved dark2 structure for 1ms delay time. The maps are shown on the dark model structure. (c) 2F_o-F_c map (at 1σ) for the model after 1 ms of photoexcitation. (d) Coordination structure of HEWL-Mn(CO)$_3$(wat)$_2$ after 17 ms of photoexcitation. (e) The difference F_{light}-F_{dark} map (at ±3.0σ, green/red) and the difference F_{light}-F_{dark} map (at ±3.0σ, green/red) against complete darkness and interleaved dark2 structure, respectively, for 17 ms delay time. The maps are shown on the dark model structure. (f) 2F_o-F_c map (at 1σ) for the model after 17 ms of photoexcitation.

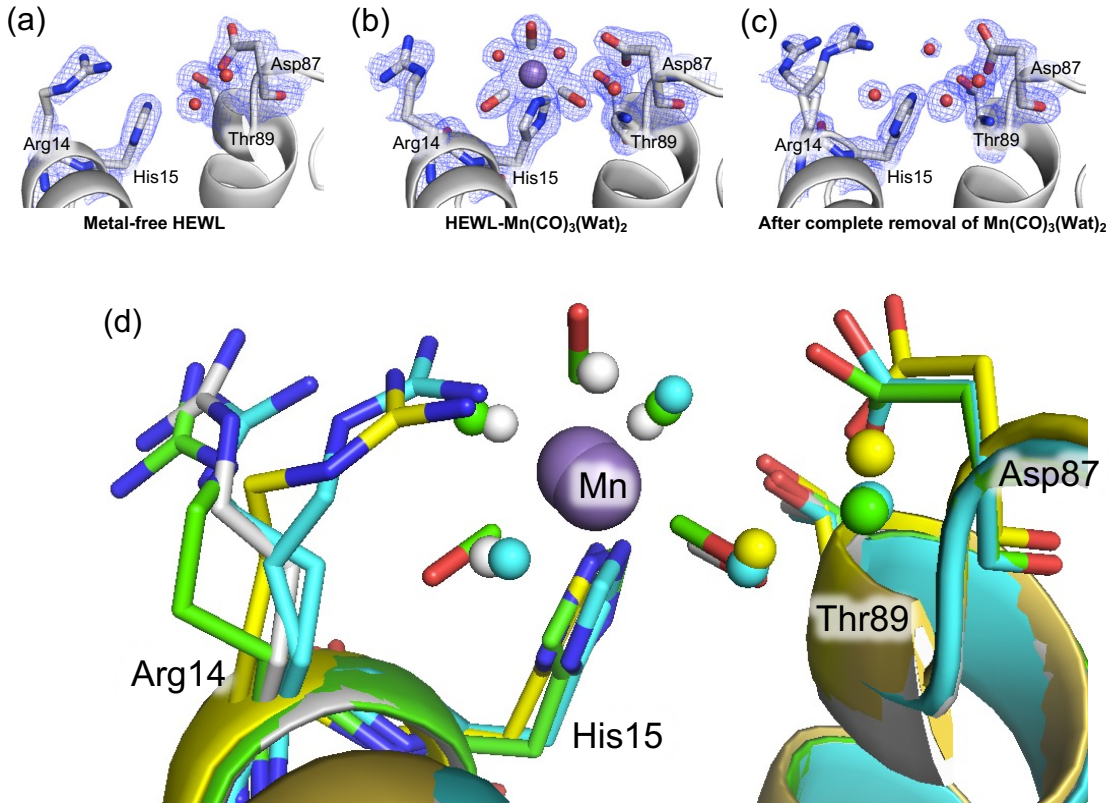

Supplementary Figure 11: Changes in the side chain residues during the CO release reaction. (a-c) Comparison of the structures of metal-free HEWL, HEWL-$Mn(CO)_3(Wat)_2$ and after complete removal of $Mn(CO)_3(Wat)_2$. Complete removal of $Mn(CO)_3(wat)_2$ was achieved by irradiating a 8W UV lamp (365nm) onto a single crystal for 20min followed by X-ray diffraction measurement at 100K in Rigaku XtalLab Synergy diffractometer. $2F_o$-F_c maps (at 1σ) are shown in blue mesh. (d) Overlap of the structure of metal-free HEWL (yellow), $Mn(CO)_3$ bounded under darkness (green), after 1μs (40μJ) of photoexcitation (grey) and after complete release of CO (cyan).

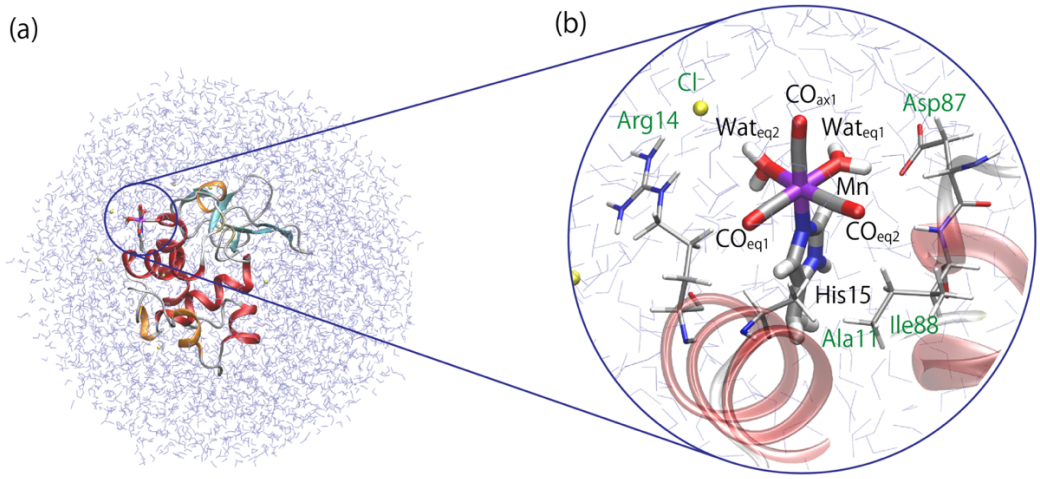

Supplementary Figure 12. Entire QM/MM system used in the present study. (a) Arrangement of HEWL in a water droplet. (b) Enlarged view for the $Mn(CO)_3(Wat)_2$ center in HEWL. Atoms in the QM region are shown in thick licorice representation.

(A)

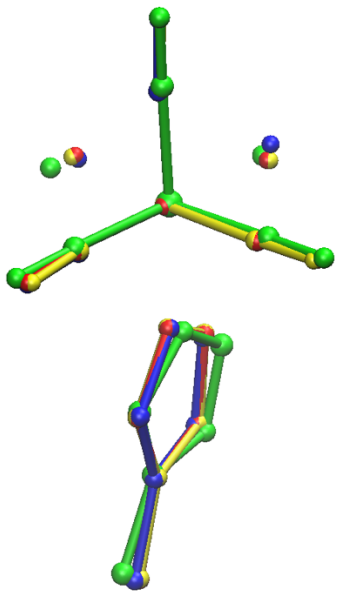

(B)

	B3LYP//DZVP[1] (B1)	B3LYP//TZVP[2] (B2)	B3LYP//TZVP+[3] (B3)	SFX (8WZF)
B1	0	0.088	0.096	0.228
B2	0.088	0	0.029	0.216
B3	0.096	0.029	0	0.216
X1	0.228	0.216	0.216	0

[1]DZVP: LANL2DZ for Mn, 6-31G* for other atoms

[2]TZVP: LANL2TZ for Mn, 6-311G* for other atoms

[3]TZVP+: LANL2TZ for Mn, 6-311+G* for other atoms

Supplementary Figure 13. (A) Superimposed structures of the Mn center by using different QM/MM method and the SFX method. Atoms are drawn with different colors: Blue for B1, Red for B2, Yellow for B3, Green for SFX. (B) Comparison of root-mean-square deviation of heavy atomic positions (RMSD) for the QM/MM optimized structures and that of the SFX crystal structure (PDBID:8WZF) in the state **1**. Different basis sets are adapted for the QM/MM optimizations. RMSD values are given in Angstrom(Å).

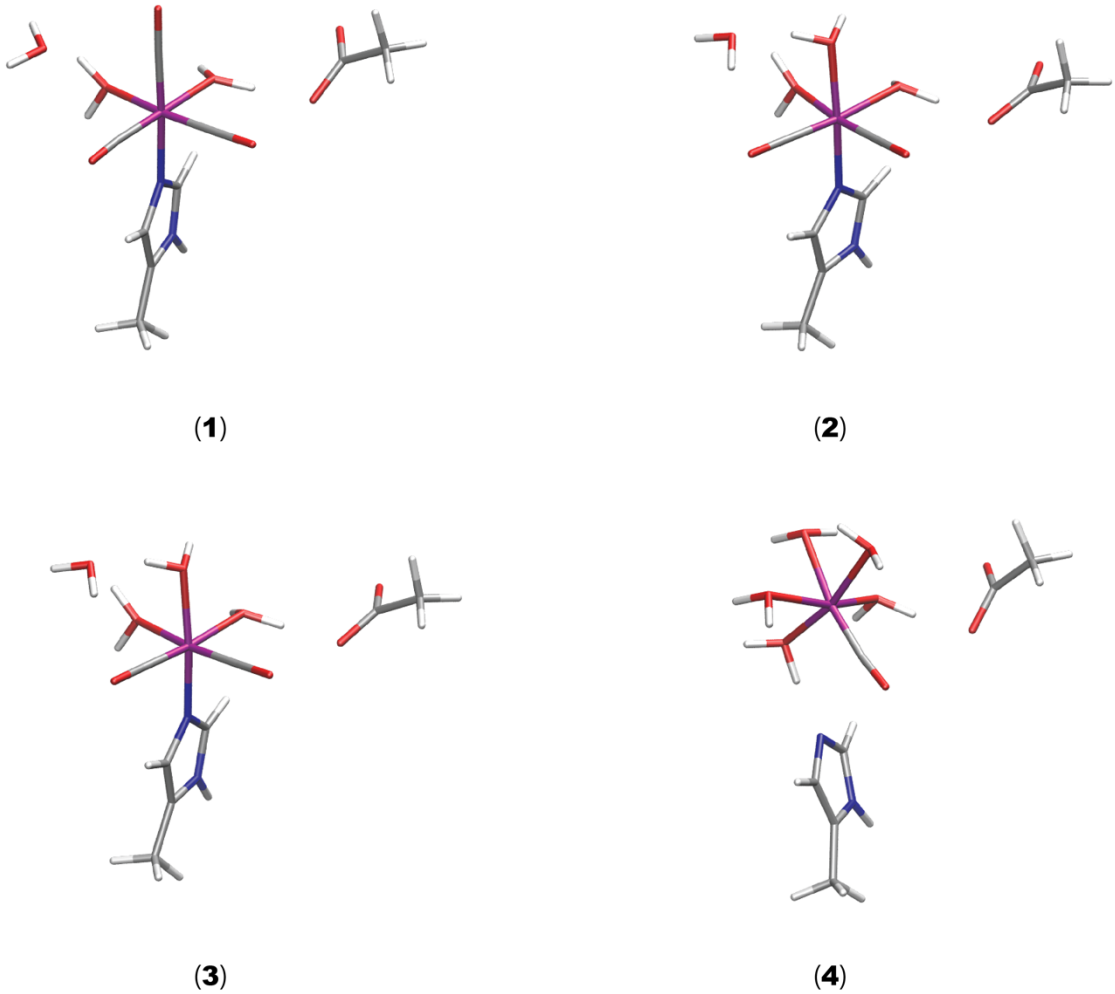

Supplementary Figure 14. Enlarged view of the QM region in the QM/MM calculations for the calculations of UV-spectra. TDDFT calculations were performed at the CAMB3LYP/TZVP+ level of theory. Calculated UV spectra were shown in Figure 5. The Asp 87 side chain was explicitly included in the QM region for the calculations of UV spectra. However, the Asp87 side chain was included in the MM region in the calculations of reaction paths to reduce the computational cost.

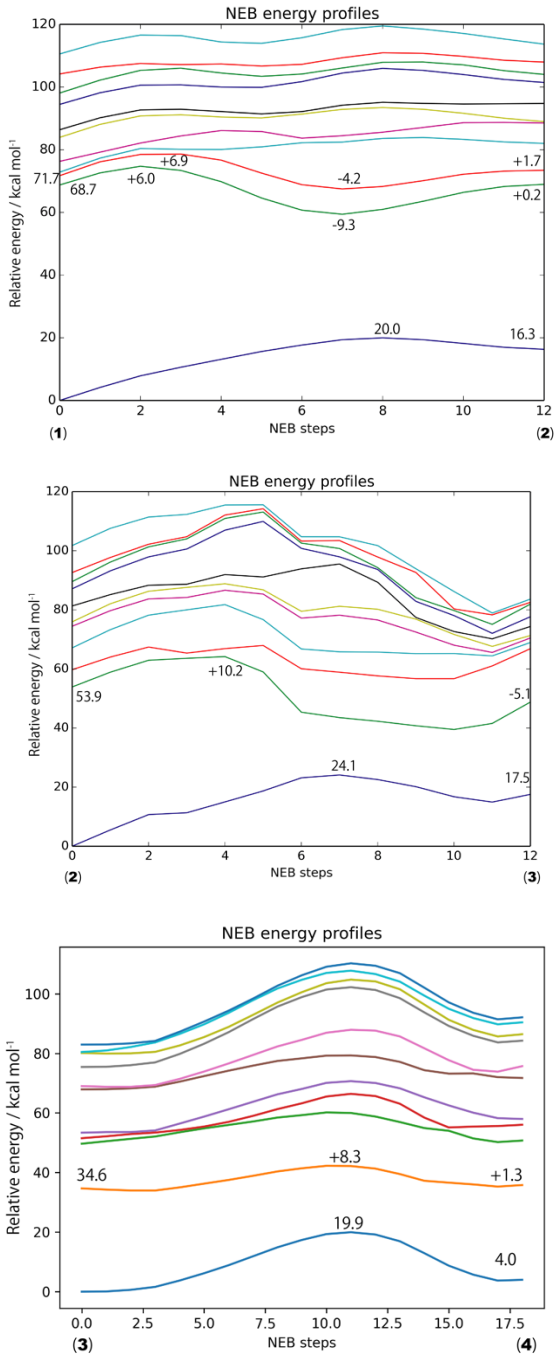

Supplementary Figure 15. NEB energy profiles along the main ligand-dissociation reactions. Relative energies are given in kcal mol^{-1}.

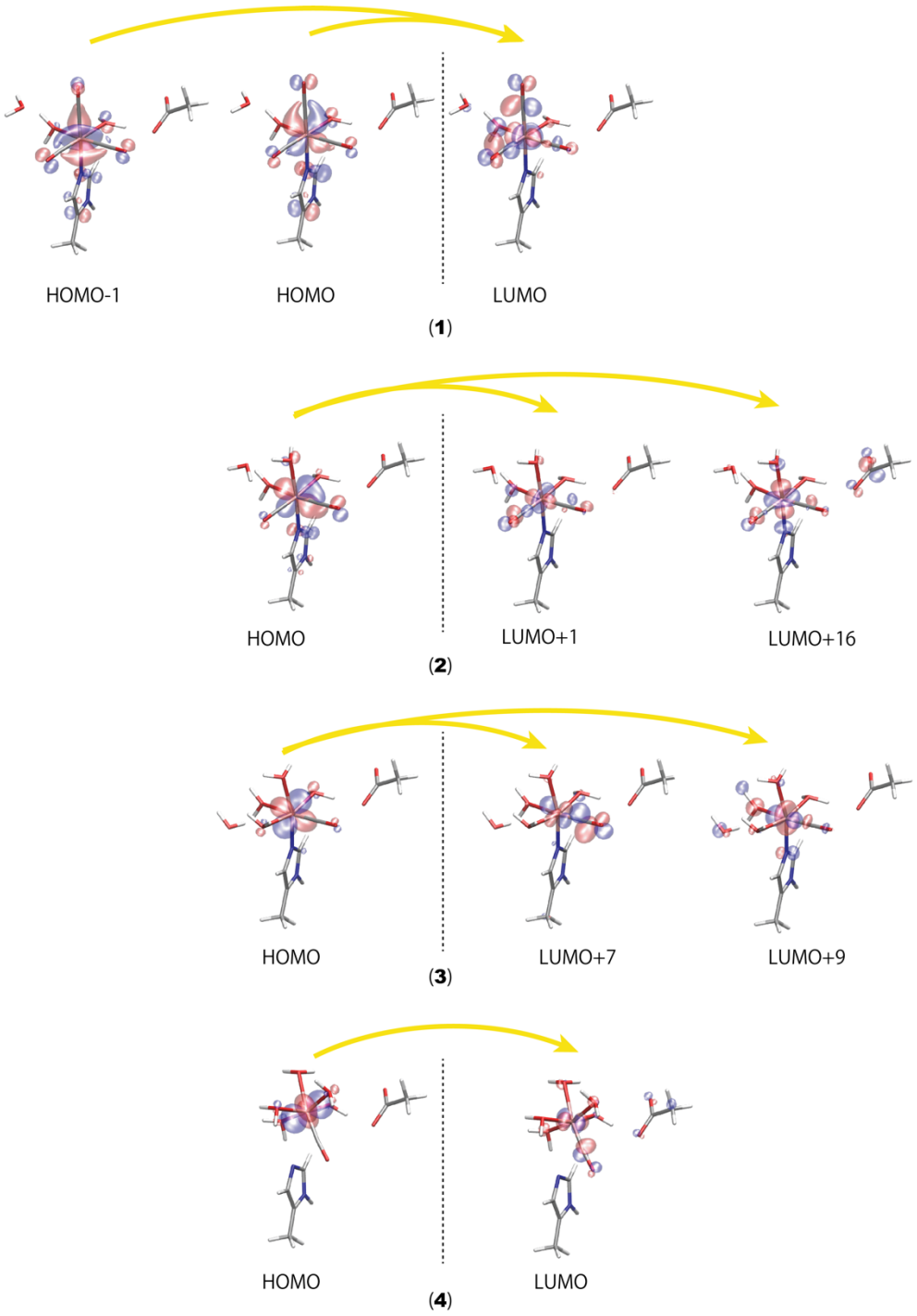

Supplementary Figure 16. Molecular orbitals mainly contribute to the first excited state calculated under the CAMB3LYP/TZVP+ level of theory. Atoms in the QM region of the QM/MM calculations are shown in Supplementary Figure 15. These HOMOs are mostly distributed on the Mn d orbitals, while the LUMOs are more delocalized to the CO and water ligands with antibonding character. These MO transitions support the ligand dissociation in these excited states.

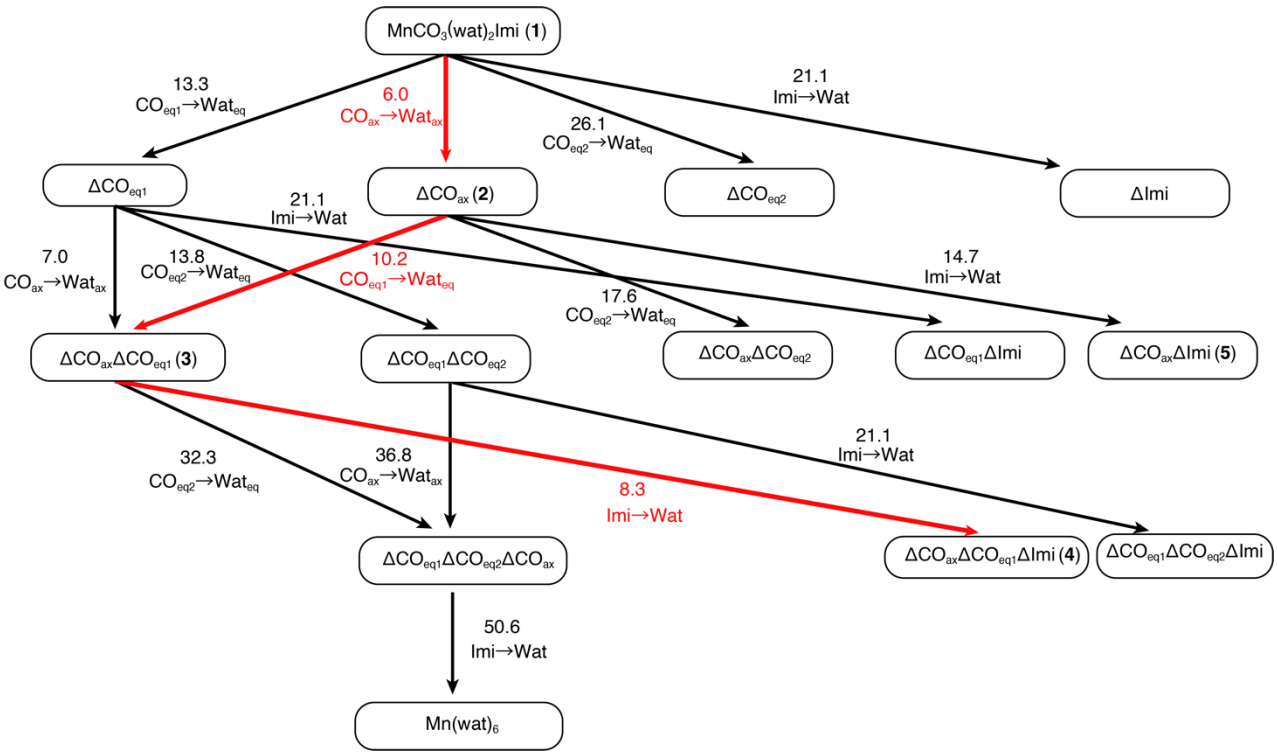

Supplementary Figure 17: Schematic representation showing the flow chart of all possible CO release steps with the energy barrier values in kcal mol^{-1} units. The corresponding ground state and excited state energies are listed in Supplementary Table 8.

Supplementary Table 1A: Crystallographic data and refinement statistics for HEWL-$Mn(CO)_3$ structures under darkness and illuminated conditions.[a]

Dataset	**Complete Darkness**	**10 ns 20 µJ**	**100 ns 20 µJ**	**1 µs 20 µJ**	**1 µs 40 µJ**
PDB code	8WZF	8WZG	8WZR	8WZT	8WZV
Data-collection date	2020/11/24	2020/11/24	2021/11/02	2021/11/02	2022/10/25
Wavelength (Å)	1.0	1.0	1.0	1.0	1.0
Space group	$P4_32_12$	$P4_32_12$	$P4_32_12$	$P4_32_12$	$P4_32_12$
Hit images	15663	16172	23627	23656	20096
Indexed images	14714	15575	22963	22882	17709
Unit cell *a, b, c* (Å); α , β , ν (°)	81.0, 81.0, 37.7; 90.0, 90.0, 90.0	81.0, 81.0, 37.7; 90.0, 90.0, 90.0	81.7, 81.7, 37.9; 90.0, 90.0, 90.0	81.7, 81.7, 37.7; 90.0, 90.0, 90.0	80.8, 80.8, 37.6; 90.0, 90.0, 90.0
Resolution range (Å)	31.44-1.60 (1.62-1.60)	31.44-1.60 (1.62-1.60)	31.64-1.60 (1.62-1.60)	31.64-1.60 (1.62-1.60)	31.44-1.60 (1.62-1.60)
Total reflections	7680482 (192494)	8081709 (190265)	14374496 (205062)	13068826 (244841)	8214252 (74168)
Unique reflections	17136 (841)	17136 (841)	17528 (859)	17528 (859)	17017 (842)
Multiplicity	448.2 (228.9)	471.6 (226.2)	820.1 (238.7)	745.6 (285.0)	482.7 (88.1)
Completeness (%)	100.0 (100.0)	100.0 (100.0)	100.0 (100.0)	100.0 (100.0)	100.0 (100.0)
Mean I/sigma (I)	6.82 (4.18)	8.04 (4.21)	9.55 (1.18)	8.54 (1.06)	8.20 (0.92)

Wilson B-factor (Å^2)	25.16	25.51	36.82	38.11	35.8
R-split	14.0 (22.7)	11.1 (21.3)	8.2 (86.4)	9.2 (90.6)	9.4 (113.8)
$CC_{1/2}$	0.965 (0.906)	0.980 (0.934)	0.990 (0.486)	0.987 (0.537)	0.987 (0.391)
Reflections used in refinement	17094	17093	17481	17483	16969
Reflections used for R-free	855	855	875	875	849
R-work (%)	19.30	18.52	19.48	19.27	19.02
R-free (%)	22.63	20.05	19.95	21.23	19.12
Number of non-hydrogen atoms	1093	1091	1095	1093	1068
Macromolecules	998	990	1020	1017	993
Ligands	9	10	7	8	5
Solvent	86	91	68	68	70
Protein residues	129	129	129	129	129
RMS deviation (bonds, Å)	0.007	0.006	0.009	0.008	0.011
RMS deviation (angles, °)	0.94	0.96	1.09	1.14	1.64
Ramachandran favored (%)	99.21	99.21	97.64	99.21	99.21
Ramachandran allowed (%)	0.79	0.79	2.36	0.79	0.79
Ramachandran outliers (%)	0	0	0	0	0

Rotamer outliers (%)	0	0	0.91	0.92	0.96
Clash score	2.03	1.03	5.44	1.49	2.05
Average B-factor (Å^2)	22.50	24.19	33.46	34.02	35.71
macromolecules (Å^2)	21.61	23.13	32.86	33.38	35.06
ligands (Å^2)	33.27	34.17	40.65	42.68	41.48
Solvent (Å^2)	31.71	34.66	41.79	42.63	44.53

Note: Values in the parentheses are for the highest-resolution shell. $R = \Sigma||F_o|-|F_c||/\Sigma|F_o|$, where F_o and F_c are the observed and calculated structure factor amplitudes, respectively. R_{free}: The R factor calculated on a partial set that is not used in the refinement of the structure. Ramachandran plot parameters were obtained from Molprobity.

[a]The data used in Figure 4c in the main text.

Supplementary Table 1B: Crystallographic data and refinement statistics for HEWL-$Mn(CO)_3$ structures under dark conditions.

Dataset	**Complete Darkness[a]**	**10 ns 20 µJ-dark2[b]**	**Complete Darkness[c]**	**100 ns 20 µJ-Dark[d]**	**1 µs 20 µJ-Dark[e]**	**Metal-free HEWL**
Data collection date	2020/11/24	2020/11/24	2021/11/02	2021/11/02	2021/11/02	2021/11/02
Wavelength (Å)	1.0	1.0	1.0	1.0	1.0	1.0
Space group	$P4_32_12$	$P4_32_12$	$P4_32_12$	$P4_32_12$	$P4_32_12$	$P4_32_12$
Hit images	33166	16903	29920	25487	25583	29731
Indexed images	30384	15968	27755	23435	23977	24491
Unit cell *a* , *b* , *c* (Å); α , β , ν (°)	81.0, 81.0, 37.7; 90.0, 90.0, 90.0	81.0, 81.0, 37.7; 90.0, 90.0, 90.0	81.7, 81.7, 37.9; 90.0, 90.0, 90.0	81.7, 81.7, 37.9; 90.0, 90.0, 90.0	81.7, 81.7, 37.9; 90.0, 90.0, 90.0	79.2, 79.2, 38.1; 90.0, 90.0, 90.0
Resolution range (Å)	31.44-1.60 (1.62-1.60)	31.44-1.60 (1.62-1.60)	31.64-1.60 (1.62-1.60)	31.64-1.60 (1.62-1.60)	31.44-1.60 (1.62-1.60)	31.54-1.60 (1.62-1.60)
Total reflections	14501712 (361248)	7942477 (192001)	15230346 (369011)	13810716 (355727)	14466062 (370389)	18189568 (517185)
Unique reflections	17136 (841)	17136 (841)	17528 (859)	17528 (859)	17528 (859)	16564 (799)
Multiplicity	846.3 (429.5)	463.5 (228.3)	868.9 (429.6)	787.9 (414.1)	825.3 (431.2)	1098.1 (647.3)
Completeness (%)	100.0 (100.0)	100.0 (100.0)	100.0 (100.0)	100.0 (100.0)	100.0 (100.0)	100.0 (100.0)
Mean I/sigma (I)	9.59 (5.57)	7.40 (4.31)	8.44 (1.41)	7.78 (1.71)	87.92 (1.59)	9.19 (3.41)
Wilson B-factor ($Å^2$)	25.21	24.77	37.14	34.74	35.2	30.69
R-split	9.50 (17.43)	12.58 (23.14)	10.27 (69.85)	11.08 (56.16)	11.04(60.48)	10.63 (28.80)
$CC_{1/2}$	0.9841 (0.9235)	0.9718 (0.8813)	0.9816 (0.6306)	0.9807(0.7056)	0.9795 (0.7003)	0.98 (0.59)

Reflections used in refinement	17094	17094	17484	17484	17485	12375
Reflections used for R-free	1220	855	875	875	875	620
R-work (%)	19.12	19.17	20.60	19.85	19.72	19.09
R-free (%)	20.75	19.94	21.58	22.43	20.40	23.10
Number of non-hydrogen atoms	1091	1094	1079	1096	1084	1082
Macromolecules	998	997	1001	1000	991	1004
Ligands	10	10	9	9	11	2
Solvent	83	87	69	87	82	76
Protein residues	129	129	129	129	129	129
RMS deviation (bonds, Å)	0.008	0.007	0.012	0.010	0.007	0.010
RMS deviation (angles, °)	0.99	1.02	1.45	1.15	0.87	0.92
Ramachandran favored (%)	99.21	99.21	97.64	99.21	98.43	99.21
Ramachandran allowed (%)	0.79	0.79	2.36	0.79	1.57	0.79
Ramachandran outliers (%)	0	0	0	0	0	0
Rotamer outliers (%)	0	0	0	0	0	0
Clash score	4.07	3.06	1.52	0.51	1.02	1.52
Average B-factor ($Å^2$)	22.13	22.56	31.08	29.33	29.50	19.48
Macromolecules ($Å^2$)	21.26	21.63	30.43	28.46	28.62	18.89

ligands (Å^2)	31.65	32.71	40.57	38.66	39.71	22.67
Solvent (Å^2)	31.52	32.06	39.30	38.31	38.77	27.19

Note: Values in the parentheses are for the highest-resolution shell. $R = \Sigma||F_o|-|F_c||/\Sigma|F_o|$, where F_o and F_c are the observed and calculated structure factor amplitudes, respectively. R_{free}: The R factor calculated on a partial set that is not used in the refinement of the structure. Ramachandran plot parameters were obtained from Molprobity.
[a]A complete darkness data used in Supplementary Figure 3 in SI. This darkness structure was collected with an interval of over 24h time to see the possibility of any dark reaction in comparison to the structure shown in Figure 3b in the main text.
[b]Interleaved dark dataset 2 for 10ns20μJ collected with 10Hz repetition.
[c,d,e]Complete darkness and interleaved dark data corresponding to datasets of delay time 100ns and 1μs as shown in Figure 4c-iii,iv. The light data were collected with 15Hz repetition.

Supplementary Table 1C: Crystallographic data and refinement statistics for HEWL-$Mn(CO)_3$ structures under selected conditions.[a]

Dataset	**Complete Darkness**	**1μs40μJ-dark2**	**1ms20μJ-light**	**1 ms20 μJ_Dark2**	**17ms20 μJ-light**	**17ms20 μJ-dark2**
Data collection date	2022/10/25	2022/10/25	2022/10/25	2022/10/25	2022/10/25	2022/10/25
Wavelength (Å)	1.0	1.0	1.0	1.0	1.0	1.0
Space group	$P4_32_12$	$P4_32_12$	$P4_32_12$	$P4_32_12$	$P4_32_12$	$P4_32_12$
Hit images	26248	25001	18547	20958	29107	31290
Indexed images	22498	20229	16909	18681	20733	21902
Unit cell *a* , *b* , *c* (Å); α , β, *ν* (°)	80.8, 80.8, 37.6; 90.0, 90.0, 90.0	80.8, 80.8, 37.6; 90.0, 90.0, 90.0	80.8, 80.8, 37.6; 90.0, 90.0, 90.0	80.8, 80.8, 37.6; 90.0, 90.0, 90.0	80.8, 80.8, 37.6; 90.0, 90.0, 90.0	80.8, 80.8, 37.6; 90.0, 90.0, 90.0
Resolution range (Å)	31.44-1.60 (1.62-1.60)	31.44-1.60 (1.62-1.60)	31.64-1.60 (1.62-1.60)	31.64-1.60 (1.62-1.60)	31.44-1.60 (1.62-1.60)	31.44-1.60 (1.62-1.60)
Total reflections	9906473 (250199)	8487553 (204454)	8324674 (125815)	7761093 (191375)	8268446 (131678)	8242297 (179195)
Unique reflections	17017 (842)	17017 (842)	17017 (842)	17017 (842)	17017 (842)	17017 (842)
Multiplicity	582.2 (297.1)	498.8 (242.8)	489.2 (149.4)	456.1 (227.3)	485.9 (156.4)	484.4 (212.8)
Completeness (%)	100.0 (100.0)	100.0 (100.0)	100.0 (100.0)	100.0 (100.0)	100.0 (100.0)	100.0 (100.0)
Mean I/sigma (I)	9.04 (3.05)	8.33 (2.48)	8.17 (1.69)	8.14 (2.50)	8.54 (1.72)	8.52 (2.17)
Wilson B-factor ($Å^2$)	31.83	32.49	32.57	32.09	33.07	32.63
R-split	10.3 (31.6)	11.2 (36.6)	10.7 (52.3)	11.3 (37.5)	10.4 (55.8)	10.8 (43.9)

$CC_{1/2}$	0.981 (0.854)	0.978 (0.839)	0.982 (0.729)	0.978 (0.821)	0.981 (0.694)	0.978 (0.799)
Reflections used in refinement	16973	16972	16971	16971	16972	16971
Reflections used for R-free	849	849	849	849	849	849
R-work (%)	19.28	19.07	18.81	19.05	18.48	18.85
R-free (%)	21.59	21.67	20.26	22.07	20.61	21.51
Number of non-hydrogen atoms	1089	1093	1095	1092	1105	1090
Macromolecules	1000	1012	1011	1012	1017	1000
Ligands	9	9	7	9	6	10
Solvent	80	77	77	71	70	80
Protein residues	129	129	129	129	129	129
RMS deviation (bonds, Å)	0.008	0.10	0.008	0.007	0.008	0.007
RMS deviation (angles, °)	1.02	1.30	1.09	0.98	1.09	0.97
Ramachandran favored (%)	99.21	99.21	97.64	99.21	98.43	98.43
Ramachandran allowed (%)	0.79	0.79	2.36	0.79	1.57	1.57
Ramachandran outliers (%)	0	0	0	0	0	0
Rotamer outliers (%)	0.94	0	0	0	0.92	0.94
Clash score	1.01	3.02	2.00	1.00	1.99	2.54
Average B-factor ($Å^2$)	27.53	29.37	31.37	28.72	31.13	29.72
Macromolecules ($Å^2$)	26.77	28.56	30.67	28.07	30.35	28.98

Ligands (Å^2)	36.64	39.22	36.36	39.17	38.47	39.56
Solvent (Å^2)	36.04	38.81	40.18	36.55	40.42	37.84

Note: Values in the parentheses are for the highest-resolution shell. $R = \Sigma||F_o|-|F_c||/\Sigma|F_o|$, where F_o and F_c are the observed and calculated structure factor amplitudes, respectively. R_{free}: The R factor calculated on a partial set that is not used in the refinement of the structure. Ramachandran plot parameters were obtained from Molprobity. [a]Complete darkness, interleaved dark2 and light data corresponding to datasets of delay time 1μs (40μJ), 1ms (20μJ) and 17ms (20μJ). The light data were collected with 10Hz repetition.

Supplementary Table 1D: Crystallographic data and refinement statistics for HEWL-$Mn(CO)_3$ structures under darkness and illuminated conditions.[a]

Dataset	**Complete Darkness**	**10 ns 10 µJ-light**	**10 ns 10 µJ - dark2**	**10 ns 20 µJ -light**	**10 ns 20 µJ -dark2**
Data collection date	2024/02/02	2024/02/02	2024/02/02	2024/02/02	2024/02/02
Wavelength (Å)	1.0	1.0	1.0	1.0	1.0
Space group	$P4_32_12$	$P4_32_12$	$P4_32_12$	$P4_32_12$	$P4_32_12$
Hit images	49363	28391	32318	28667	35894
Indexed images	44114	25120	26505	25693	29076
Unit cell	80.7, 80.7, 37.5;	80.7,80.7,37.5;	80.7,80.7,37.5;	80.7,80.7,37.5	80.7,80.7,37.5;
a, b, c (Å);	90.0, 90.0, 90.0	90.0,90.0,90.0	90.0,90.0,90.0	90.0,90.0,90.0	90.0,90.0,90.0
α , β , ν (°)					
Resolution range (Å)	40.32-1.60	40.32-1.60	40.32-1.60	40.32-1.60	40.32-1.60
	(1.62-1.60)	(1.62-1.60)	(1.62-1.60)	(1.62-1.60)	(1.62-1.60)
Total reflections	16656640 (525574)	12995801 (341995)	8436123 (250921)	16770074 (369630)	9605810 (290361)
Unique reflections	16936 (843)	16936 (843)	16936 (843)	16936 (843)	16936 (843)
Multiplicity	983.5 (623.50)	767.3 (405.70)	498.1 (297.70)	16936 (843)	567.2 (344.40)
Completeness (%)	100.0 (100.00)	100.0(100.00)	100.0 (100.0)	100.0 (100.0)	100.0 (100.0)
Mean I/sigma (I)	13.03 (6.33)	12.42 (3.50)	10.24 (4.62)	12.59 (2.58)	10.56 (4.96)
Wilson B-factor ($Å^2$)	27.48	27.94	27.81	28.63	27.82
R-split	7.7 (15.46)	7.5 (28.45)	10.2 (19.54)	7.0 (38.60)	10.0 (18.21)

$CC_{1/2}$	0.990 (0.9131)	0.991 (0.9008)	0.981 (0.9434)	7.0 (38.60)	0.982 (0.9455)
Reflections used in refinement	20383	16888	20380	20375	20381
Reflections used for R-free	1020	845	1019	1019	1019
R-work (%)	18.66	17.68	18.43	18.18	18.35
R-free (%)	21.32	0.1985	20.25	21.39	20.42
Number of non-hydrogen atoms	1136	1115	1131	1112	1138
Macromolecules	1012	1006	1012	1006	1012
Ligands	11	9	11	9	11
Solvent	113	100	108	97	115
Protein residues	129	129	129	129	129
RMS deviation (bonds, Å)	0.007	0.006	0.007	0.007	0.007
RMS deviation (angles, °)	1.00	0.94	0.96	0.91	0.98
Ramachandran favored (%)	99.21	99.21	99.21	99.21	99.21
Ramachandran allowed (%)	0.79	0.79	0.79	0.79	0.79
Ramachandran outliers (%)	0	0	0	0	0

Rotamer outliers (%)	0	0	0	0	0
Clash score	0.50	1.01	1.00	2.01	1.50
Average B-factor (Å^2)	25.74	25.36	26.62	28.38	26.70
macromolecules (Å^2)	24.40	24.12	25.27	27.20	25.26
ligands (Å^2)	36.79	38.38	38.11	41.29	38.37
Solvent (Å^2)	36.68	36.70	38.08	39.44	38.25

Note: Values in the parentheses are for the highest-resolution shell. $R = \Sigma||F_o|-|F_c||/\Sigma|F_o|$, where F_o and F_c are the observed and calculated structure factor amplitudes, respectively. R_{free}: The R factor calculated on a partial set that is not used in the refinement of the structure. Ramachandran plot parameters were obtained from Molprobity.

[a]The data used in Supplementary Figure 9A in SI.

Supplementary Table 1E: Crystallographic data and refinement statistics for HEWL-$Mn(CO)_3$ structures under darkness and illuminated conditions.[a]

Dataset	**10 ns 40 µJ-light**	**10 ns 40 µJ-dark2**	**1 µs 10 µJ-light**	**1 µs 10 µJ-dark2**	**1 µs 20 µJ-light**
Data collection date	2024/02/02	2024/02/02	2024/02/02	2024/02/02	2024/02/02
Wavelength (Å)	1.0	1.0	1.0	1.0	1.0
Space group	$P4_32_12$	$P4_32_12$	$P4_32_12$	$P4_32_12$	$P4_32_12$
Hit images	25228	33368	30958	33713	29190
Indexed images	23365	27717	21340	21635	25856
Unit cell *a, b, c* (Å); α , β , ν (°)	80.7,80.7,37.5; 90.0,90.0,90.0	80.7,80.7,37.5; 90.0,90.0,90.0	80.7,80.7,37.5; 90.0,90.0,90.0	80.7,80.7,37.5; 90.0,90.0,90.0	80.7,80.7,37.5; 90.0,90.0,90.0
Resolution range (Å)	40.32-1.60 (1.62-1.60)	40.32-1.60 (1.62-1.60)	40.32-1.60(1.62-1.60)	40.32-1.60(1.62-1.60)	40.32-1.60(1.62-1.60)
Total reflections	19749625 (417750)	10460471 (332872)	9124629 (278247)	8153584 (258037)	13734938 (399769)
Unique reflections	16936 (843)	16936 (843)	16936 (843)	16936 (843)	16936 (843)
Multiplicity	1166.1 (495.60)	617.6 (394.90)	538.8 (330.10)	16936 (843)	811.0 (474.20)
Completeness (%)	100.0 (100.0)	100.0 (100.0)	100.0 (100.0)	100.0 (100.0)	100.0 (100.00)
Mean I/sigma (I)	12.25 (1.66)	10.57 (5.28)	9.90 (3.95)	9.28 (4.92)	11.10 (2.75)
Wilson B-factor ($Å^2$)	30.96	27.31	28.65	27.33	30.84
R-split	6.2 (62.99)	9.7 (16.58)	10.0 (22.99)	11.0 (19.19)	7.7 (38.86)
$CC_{1/2}$	6.2 (62.99)	0.984 (0.9586)	0.982 (0.9270)	11.0 (19.19)	0.991 (0.5649)

Reflections used in refinement	20336	20384	20379	20379	16882
Reflections used for R-free	1019	1020	1019	1019	845
R-work (%)	18.16	18.85	18.97	19.28	18.21
R-free (%)	21.10	21.09	22.90	22.15	21.89
Number of non-hydrogen atoms	1095	1133	1117	1139	1109
Macromolecules	1006	1012	1006	1012	1006
Ligands	7	11	11	11	7
Solvent	82	110	100	116	96
Protein residues	129	129	129	129	129
RMS deviation (bonds, Å)	0.006	0.007	0.006	0.013	0.006
RMS deviation (angles, °)	0.91	0.93	0.96	1.61	0.91
Ramachandran favored (%)	98.43	99.21	99.21	98.43	99.21
Ramachandran allowed (%)	1.57	0.79	0.79	1.57	0.79
Ramachandran outliers (%)	0	0	0	0	0

Rotamer outliers (%)	0	0	0	0	0
Clash score	0.50	1.50	2.51	1.00	2.52
Average B-factor ($Å^2$)	31.25	25.57	26.59	25.43	28.36
macromolecules ($Å^2$)	30.32	24.23	25.42	24.08	27.32
ligands ($Å^2$)	40.24	36.97	40.10	35.40	35.82
Solvent ($Å^2$)	41.89	36.76	36.87	36.31	38.66

Note: Values in the parentheses are for the highest-resolution shell. $R = \Sigma||F_o|-|F_c||/\Sigma|F_o|$, where F_o and F_c are the observed and calculated structure factor amplitudes, respectively. R_{free}: The R factor calculated on a partial set that is not used in the refinement of the structure. Ramachandran plot parameters were obtained from Molprobity.

[a]The data used in Supplementary Figure 9 in SI.

Supplementary Table 1F: Crystallographic data and refinement statistics for HEWL-$Mn(CO)_3$ structures under darkness and illuminated conditions.[a]

Dataset	**1 µs 20 µJ-dark2**	**1 µs 40 µJ-light**	**1 µs 40 µJ-dark2**	**1 µs 60 µJ-light**	**1 µs 60 µJ-dark2**
Data collection date	2024/02/02	2024/02/02	2024/02/02	2024/02/02	2024/02/02
Wavelength (Å)	1.0	1.0	1.0	1.0	1.0
Space group	$P4_32_12$	$P4_32_12$	$P4_32_12$	$P4_32_12$	$P4_32_12$
Hit images	33052	24139	31218	27168	46021
Indexed images	27959	21650	26687	21398	36187
Unit cell	80.7,80.7,37.5;	80.7,80.7,37.5;	80.7,80.7,37.5;	80.7,80.7,37.5;	80.7,80.7,37.5;
a, b, c (Å);	90.0,90.0,90.0	90.0,90.0,90.0	90.0,90.0,90.0	90.0,90.0,90.0	90.0,90.0,90.0
α , β , ν (°)					
Resolution range (Å)	40.32-1.60(1.62-1.60)	40.32-1.60(1.62-1.60)	40.32-1.60(1.62-1.60)	40.32-1.70 (1.72-1.70)	40.32-1.60 (1.62-1.60)
Total reflections	10621158 (333069)	13016895 (257223)	9672291 (294456)	12818802 (291013)	13445059 (423947)
Unique reflections	16936 (843)	16936 (843)	16936 (843)	14190 (693)	16936 (843)
Multiplicity	627.1 (395.10)	768.6 (305.10)	571.1 (349.30)	14190 (693)	793.9 (502.90)
Completeness (%)	100.0 (100.0)	100.0 (100.0)	100.0 (100.0)	100.0 (100.0)	100.0 (100.00)
Mean I/sigma (I)	10.56 (5.22)	8.91 (1.19)	9.98 (4.72)	9.89 (1.32)	793.9 (502.90)

Wilson B-factor (Å^2)	27.28	32.31	27.31	34.44	27.53
R-split	9.9 (16.84)	8.5 (81.28)	10.6 (18.64)	7.8 (79.32)	8.5 (14.71)
$CC_{1/2}$	0.980 (0.9564)	0.991(0.5155)	0.982 (0.9442)	0.992 (0.5088)	0.987 (0.9699)
Reflections used in refinement	16886	16884	16891	14138	16886
Reflections used for R-free	845	845	845	706	845
R-work (%)	18.35	18.19	19.68	19.08	18.88
R-free (%)	18.86	20.56	20.15	21.83	21.61
Number of non-hydrogen atoms	1140	1086	1130	1093	1135
Macromolecules	1012	1006	1010	1006	1012
Ligands	11	5	12	6	11
Solvent	117	75	108	81	112
Protein residues	129	129	129	129	129
RMS deviation (bonds, Å)	0.007	0.006	0.013	0.012	0.013
RMS deviation (angles, °)	0.99	1.00	1.77	1.66	1.63
Ramachandran favored (%)	99.21	98.43	97.64	98.43	98.43

Ramachandran allowed (%)	0.79	1.57	2.36	1.57	1.57
Ramachandran outliers (%)	0	0	0	0	0
Rotamer outliers (%)	0	0	0	0.94	0
Clash score	1.00	2.52	0	4.54	2.50
Average B-factor ($Å^2$)	23.94	32.32	21.76	32.91	22.99
macromolecules ($Å^2$)	22.38	31.58	20.32	32.14	21.62
ligands ($Å^2$)	35.21	39.19	32.70	41.37	34.17
Solvent ($Å^2$)	36.33	41.73	34.03	41.97	34.31

Note: Values in the parentheses are for the highest-resolution shell. $R = \Sigma||F_o|-|F_c||/\Sigma|F_o|$, where F_o and F_c are the observed and calculated structure factor amplitudes, respectively. R_{free}: The R factor calculated on a partial set that is not used in the refinement of the structure. Ramachandran plot parameters were obtained from Molprobity.

[a]The data used in Supplementary 9 in SI.

Supplementary Table 2: Selected bond angles and bond distances in the coordination structure of $Mn(CO)_3(wat)_2$ bounded by His15 in complete darkness structure.[a]

Bond distances (Å)		Bond angles (°)	
Mn-N$^{\varepsilon}$(His15)	2.26	C(CO_{ax})-Mn-N$^{\varepsilon}$(His15)	174.01
Mn-O(wat_{eq1})	2.15	C(CO_{eq1})-Mn-O(wat_{eq1})	173.51
Mn-O(wat_{eq2})	2.33	C(CO_{eq2})-Mn-O(wat_{eq4})	177.95
Mn-C(CO_{eq1})	1.94	Mn-C(CO_{eq1})-O(CO_{eq1})	178.05
Mn-C(CO_{eq2})	1.93	Mn-C(CO_{eq2})-O(CO_{eq2})	174.86
Mn-C(CO_{ax})	1.94	Mn-C(CO_{ax})-O(CO_{ax})	174.95
C-O(CO_{eq1})	1.19	wat_{eq1}-Mn-wat_{eq2}	85.69
C-O(CO_{eq2})	1.19	Wat_{eq2}-Mn-C(CO_{eq1})	88.17
C-O(CO_{ax})	1.19	C(CO_{eq2})-Mn-wat_{eq1}	94.51
O(wat_{eq1})-O$^{\nu}$ (Asp87)	2.74	C(CO_{eq1})-Mn-C(CO_{eq2})	91.55
O(wat_{eq1})-O$^{\delta}$ (Thr89)	3.14	Wat_{eq1}-Mn- N$^{\varepsilon}$(His15)	78.45
O(wat_{eq2})-N$^{\varepsilon}$ (Arg14)	3.90	Wat_{eq2}-Mn- N$^{\varepsilon}$(His15)	82.76

[a]The data corresponds to the structure shown in Figure 3b. The bond distances and angles are measured using pymol.

Supplementary Table 3: Occupancy and B-factors (Å^2) of selected atoms in HEWL-Mn(CO)$_3$(wat)$_2$ at various conditions, with structures refined using a single model structure.

	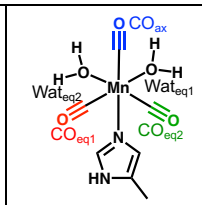	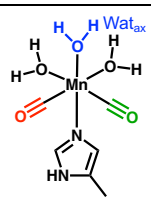	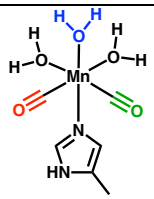	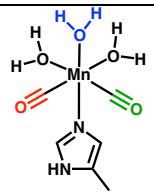	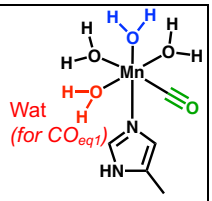
	Darkness	**10 ns20 µJ**	**100 ns20 µJ**	**1 µs20 µJ**	**1 µs40 µJ**
	B-fact. (Occu.)[a]	**B-fact. (Occu.)**[a]	**B-fact. (Occu.)**[a]	**B-fact. (Occu.)**[a]	**B-fact. (Occu.)**[a]
N$^{\varepsilon 2}$ (His15)	30.88 (1.0)	31.12 (1.0)	41.60 (1.0)	42.88 (1.0)	45.60 (1.0)
Mn	30.25 (1.0)	31.53 (0.9)	42.04 (0.9)	41.77 (0.85)	44.14 (0.65)
CO$_{eq1}$, C	30.56 (1.0)	29.98 (0.9)	40.58 (0.9)	43.21 (0.85)	45.53 (0.65)
CO$_{eq1}$, O	36.50 (1.0)	36.60 (0.9)	47.00 (0.9)	49.11 (0.85)	**(Wat)**
CO$_{eq2}$, C	30.20 (1.0)	31.70 (0.9)	38.83 (0.9)	40.81 (0.85)	40.91 (0.65)
CO$_{eq2}$, O	34.16 (1.0)	34.23 (0.9)	41.41 (0.9)	41.86 (0.85)	44.45 (0.65)
CO$_{ax}$, C	35.10 (1.0)	35.12 (0.9)	44.42 (0.9)	44.01 (0.85)	46.85 (0.65)
CO$_{ax}$, O	41.42 (1.0)	**(Wat$_{ax}$)**	**(Wat$_{ax}$)**	**(Wat$_{ax}$)**	**(Wat$_{ax}$)**
Wat$_{eq1}$	31.44 (1.0)	33.83 (0.9)	46.38 (0.9)	45.12 (0.85)	48.50 (0.65)
Wat$_{eq2}$	38.84 (1.0)	39.51 (0.9)	51.16 (0.9)	50.51 (0.85)	52.09 (0.65)
Average B-factor[b]					
Main chain	19.61	21.23	30.37	30.97	33.18
Side chain	23.76	25.19	35.42	35.88	37.10
His15	28.20	28.80	39.40	40.02	43.60
Mn-unit[c]	34.27	34.06	43.98	44.55	46.07

[a]B-factor (Å^2) and occupancy refinement: At the initial stage of model building, both B-factor and occupancy were allowed to refine freely in "Phenix refine". Finally, the occupancy of Mn ion was adjusted a little manually to have the B-factor close to the surrounding (N$^{\varepsilon 2}$ of His15). The occupancy of other coordinating ligands was kept same as Mn.

[b]The average B-factors of all protein side-chain, main-chain, His15 (side-chain) and Mn-unit were obtained from B-average in CCP4.

[c]Mn-unit represents the Mn ion with all coordinating ligands (wat or CO) except His15.

Supplementary Table 4. Measured changes in the difference density features during power titration.

	Δt = 10 ns			Δt = 1 µs			
	10 µJ	20 µJ	40 µJ	10 µJ	20 µJ	40 µJ	60 µJ
Scale e.Å^{-3}/σ	0.039	0.046	0.054	0.036	0.043	0.056	0.064
Mn	6.0 (0.235)	10.7 (0.495)	11.6 (0.626)	6.3 (0.237)	11.7 (0.497)	12.4 (0.692)	13.8 (0.884)
CO_{ax} σ (e.Å^{-3})	2.9 (0.114)	4.3 (0.199)	4.6 (0.246)	2.9 (0.109)	4.5 (0.191)	4.8 (0.268)	5.0 (0.327)
CO_{eq1} σ (e.Å^{-3})	0	1.9 (0.088)	2.5 (0.135)	0	2.4 (0.102)	4.0 (0.223)	3.6 (0.224)
CO_{eq2} σ (e.Å^{-3})	0	0	0	0	1.6 (0.066)	2.4 (0.134)	3.0 (0.186)

The values were obtained from the COOT visualization. For complete dark data, the difference density features are considered as zero. Δt is the delay time.

Supplementary Table 5. Comparison of bond distances (Å) around the Mn center between SFX and QM/MM results for species involved in the photoreaction.

	$MnCO_{ax}CO_{eq1}$ $CO_{eq2}Wat_2Im$ (**1**)	$MnWat_{ax}CO_{eq1}$ $CO_{eq2}Wat_2Im$ (**2**)	$MnWat_{ax}Wat_{eq1}$ $CO_{eq2}Wat_2Im$ (**3**)	Complete darkness **8WZF**	10ns 20μJ **8WZG**	1μs 40μJ **8WZV**
Mn-C@CO_{ax}	1.84			1.94		
Mn-O@Wat_{ax}		2.12	2.15		2.35	2.17
Mn-C@CO_{eq1}	1.81	1.78		1.94	1.94	
Mn-O@Wat_{eq1}			2.13			2.26
Mn-C@CO_{eq2}	1.79	1.77	1.76	1.93	1.94	1.95
Mn-O@Wat_{eq2}						
Mn-O@Wat_{wat1}	2.13	2.12	2.11	2.15	2.19	2.15
Mn-O@Wat_{wat2}	2.12	2.16	2.25	2.33	2.24	2.33
Mn-N@Im	2.12	2.07	2.07	2.26	2.22	2.45

Supplementary Table 6. Root-mean-square deviation (RMSD) of the Mn center among the QM/MM optimized structures and SFX structures. RMSD values are given in Angstrom(Å). The smallest values in comparisons with QM/MM and SFX results are underlined.

	$MnCO_{ax}CO_{eq1}$ $CO_{eq2}Wat_2Im$ **1**	$MnWat_{ax}CO_{eq1}$ $CO_{eq2}Wat_2Im$ **2**	$MnWat_{ax}Wat_{eq1}$ $CO_{eq2}Wat_2Im$ **3**	Complete darkness **8WZF**	10ns 20μJ **8WZG**	1μs 40μJ **8WZV**
1	0	0.108	0.157	<u>0.209</u>	0.281	0.398
2	0.108	0	0.146	<u>0.240</u>	0.250	0.394
3	0.157	0.146	0	<u>0.237</u>	0.257	0.374
8WZF	<u>0.209</u>	0.240	0.237	0	0.178	0.294
8WZG	0.281	<u>0.250</u>	0.257	0.178	0	0.218
8WZV	0.398	0.394	<u>0.374</u>	0.294	0.218	0

Supplementary Table 7. Comparison of the peak-top of absorption spectra in state **1** by using QM/MM methods with the experimental result. Different DFT functional, basis sets and QM region are adapted for the QM/MM methods.

Entry	(QM level for excited states: DFT functional/basis set, QM region)@ (QM level for the ground state calculation)	Peak-top / nm	Energy of the first excited state /eV (kcal)
1	B3LYP/DZVP, Mn center @B1	387	3.007 (69.3)
2	B3LYP/TZVP, Mn center @B1	384	3.025 (69.7)
3	B3LYP/TZVP+, Mn center @B1	386	3.009 (69.3)
4	CAM-B3LYP/DZVP, Mn center @B1	392	2.969 (68.4)
5	CAM-B3LYP/TZVP, Mn center @B1	388	2.998 (69.1)
6	CAM-B3LYP/TZVP+, Mn center @B1	389	2.983 (68.7)
7	CAM-B3LYP/DZVP, Mn center+Asp87 @B1 (QM: Mn center+Asp87)	397	2.963 (68.3)
8	CAM-B3LYP/TZVP, Mn center+Asp87 @B1(QM: Mn center+Asp87)	392	2.992 (68.9)
9	CAM-B3LYP/TZVP+, Mn center+Asp87 @B1(QM: Mn center+Asp87)	394	2.978 (68.6)
10	CAM-B3LYP/DZVP, Mn center+Asp87 @B2 (QM: Mn center+Asp87)	396	2.934 (67.6)
11	CAM-B3LYP/TZVP, Mn center+Asp87 @B2(QM: Mn center+Asp87)	392	2.967 (68.4)
12	CAM-B3LYP/TZVP+, Mn center+Asp87 @B2(QM: Mn center+Asp87)	394	2.952 (68.1)
10	Exp.	395	

Table S8. Energy differences (D*E* / kcal mol^{-1}) during the ligand-Water exchange reactions in HEWL-Mn(CO)$_n$Wat$_m$ calculated by using the NEB method. Each reaction pathway is optimized in the ground state (S_0).

Index	Reaction Step	D$E^{\neq}$(ex) [a]	D$E^{\neq}$(g) [b]	D*E* (g) [c]
1	$Mn(CO)_3Wat_{eq1}\underline{Wat_{eq2}}Im$ (**1**) + **Wat** → $Mn(CO)_3Wat_{eq1}$**Wat**Im + $\underline{Wat_{eq2}}$	3.2	13.9	0
2	$Mn(CO)_2\underline{CO_{ax}}Wat_2Im$ + **Wat** → $Mn(CO)_2$**Wat**Wat_2Im (**2**) + $\underline{CO_{ax}}$	6.0	20.0	16.3
3	$Mn\underline{CO_{eq1}}(CO)_2Wat_2Im$ + **Wat** → Mn**Wat**$(CO)_2Wat_2Im$ + $\underline{CO_{eq1}}$	2.2 (13.3)	21.9	18.9
4	$Mn\underline{CO_{eq2}}(CO)_2Wat_2Im$ + **Wat** → Mn**Wat**$(CO)_2Wat_2Im$ + $\underline{CO_{eq2}}$	26.1	30.3	1.7
5	$Mn(CO)_3Wat_2\underline{Im}$ + **Wat** → $Mn(CO)_3Wat_2$**Wat** + $\underline{Im}$	21.1	22.5	16.0
6	$Mn\underline{CO_{eq1}}CO_{eq2}Wat_{ax}Wat_2Im$ (**3**) + **Wat** → Mn**Wat**$CO_{eq2}Wat_{ax}Wat_2Im$ + $\underline{CO_{eq1}}$	10.2	24.1	17.5
7	$MnCO_{eq1}\underline{CO_{eq2}}Wat_{ax}Wat_2Im$ + **Wat** → $MnCO_{eq1}$**Wat**$Wat_{ax}Wat_2Im$ + $\underline{CO_{eq2}}$	17.6	27.6	0.5
8	$Mn(CO)_2Wat_{ax}Wat_2\underline{Im}$ + **Wat** → $Mn(CO)_2Wat_{ax}Wat_2$**Wat** (**5**) + $\underline{Im}$	-2.9 (14.7)	26.9	22.0
9	$MnWat_{eq1}CO_{eq2}\underline{CO_{ax}}Wat_2Im$ + **Wat** → $MnWat_{eq1}CO_{eq2}$**Wat**Wat_2Im + $\underline{CO_{ax}}$	4.7 (7.0)	21.1	19.6
10	$MnWat_{eq1}\underline{CO_{eq2}}CO_{ax}Wat_2Im$ + **Wat** → $MnWat_{eq1}$**Wat** $CO_{ax}Wat_2Im$ + $\underline{CO_{eq2}}$	13.8	32.0a	7.5
11	$MnWat_{eq1}CO_{eq2}CO_{ax}Wat_2\underline{Im}$ + **Wat** → $MnWat_{eq1}CO_{eq2}CO_{ax}Wat_2$**Wat** + $\underline{Im}$	21.1	26.3	17.2
12	$MnWat_2\underline{CO_{ax}}Wat_2Im$ + **Wat** → $MnWat_2$**Wat**Wat_2Im + $\underline{CO_{ax}}$	36.8	41.9	39.4
13	$MnWat_2CO_{ax}Wat_2\underline{Im}$ + **Wat** → $MnWat_2CO_{ax}Wat_2$**Wat** + $\underline{Im}$	21.1	40.8	31.1
14	$MnWat_{eq1}\underline{CO_{eq2}}Wat_{ax}Wat_2Im$ + **Wat** → $MnWat_{eq1}$**Wat**$Wat_{ax}Wat_2Im$ + $\underline{CO_{eq2}}$	32.3	46.5	33.0
15	$MnWat_{eq1}Wat_{eq2}CO_{ax}Wat_2\underline{Im}$ + **Wat** → $MnWat_{eq1}Wat_{eq2}CO_{ax}Wat_2$**Wat** (**4**) + $\underline{Im}$	8.3	19.9	4.0
16	$MnWat_{eq1}Wat_{eq2}Wat_{ax}Wat_2\underline{Im}$ + **Wat** → $MnWat_{eq1}Wat_{eq2}Wat_{ax}Wat_2$**Wat** + $\underline{Im}$	50.6	42.7	33.4

[a] Activation barrier in the first excited state along the ligand-water exchange reaction. Values in parenthesis are additional activation barrier in the ground state after the state transition from the first excited state to the ground state in the relaxation process.

[b] Activation barrier in the ground state along the ligand-water exchange reaction.

[c] Energy difference of the product state relative to the reactant state.

Supplementary Table 9: Atomic coordinates of the QM region in the intermediate states are provided in the XYZ format and in Å units. All the results are optimized at the B3LYP//DZVP level of theory in the QM/MM model used for the NEB calculations.

28			
Mn CO3 Wat3 Im (1)			
C	8.338996	-5.054998	10.908995
H	8.662996	-5.136998	9.869995
H	7.498996	-4.360998	10.963995
C	7.940996	-6.418997	11.388995
N	8.443996	-7.557996	10.782995
H	9.054996	-7.543996	9.964995
C	7.952996	-8.643996	11.421995
H	8.166996	-9.659995	11.149995
N	7.147997	-8.275996	12.413994
C	7.134997	-6.888997	12.400994
H	6.556997	-6.340997	13.123994
C	5.751997	-8.300996	14.912993
C	4.488998	-9.324996	12.918994
C	5.375997	-10.878995	14.805993
O	5.460997	-7.442996	15.625993
O	3.458998	-9.223996	12.401994
O	4.930998	-11.696994	15.475993
Mn	6.095997	-9.597995	13.690994
O	8.058996	-10.154995	14.276993
H	8.737996	-9.474996	14.117993
H	8.267996	-10.549995	15.152993
O	6.403997	-11.104995	12.237994
H	5.788997	-11.221995	11.451995
H	7.209997	-11.635995	12.129994
O	6.563997	-9.793995	17.391992
H	6.761997	-9.090996	18.062991
H	7.293997	-10.429995	17.502992
C	9.506996	-4.467998	11.738994
28			
del COax (2)			
C	8.344996	-5.032998	10.894995
H	8.678996	-5.121998	9.860995
H	7.505996	-4.331998	10.936995
C	7.935996	-6.402997	11.351995
N	8.451996	-7.519996	10.717995
H	9.057996	-7.470996	9.894995
C	8.000996	-8.622996	11.352995
H	8.257996	-9.624995	11.066995
N	7.207997	-8.282996	12.362994
C	7.158997	-6.898997	12.367994
H	6.580997	-6.368997	13.103994
C	5.911997	-8.312996	14.906993
C	4.698998	-9.322996	13.055994
C	3.678998	-12.263994	13.699994
O	5.488997	-7.517996	15.635993
O	3.650998	-9.129996	12.582994
O	2.714999	-12.107994	13.115994
Mn	6.331997	-9.574995	13.705994
O	8.392996	-10.068995	14.208993
H	9.047996	-9.361996	14.053993
H	8.674996	-10.507995	15.045993
O	6.472997	-11.254995	12.346994

28			
del COeq1			
C	8.331996	-5.067998	10.917995
H	8.637996	-5.138998	9.873995
H	7.479996	-4.385998	10.980995
C	7.962996	-6.453997	11.382995
N	8.534996	-7.550996	10.755995
H	9.137996	-7.484996	9.937995
C	8.092996	-8.674996	11.350995
H	8.369996	-9.667995	11.043995
N	7.252997	-8.378996	12.338994
C	7.165997	-6.991997	12.369994
H	6.543997	-6.494997	13.096994
C	3.408998	-10.487995	15.497993
C	4.702998	-9.570995	12.852994
C	5.841997	-11.291995	14.502993
O	3.857998	-9.744995	16.238992
O	3.651998	-9.349996	12.404994
O	5.613997	-12.319994	14.994993
Mn	6.328997	-9.844995	13.534994
O	8.271996	-9.812995	14.567993
H	9.054996	-9.447996	14.116993
H	8.596996	-10.466995	15.233993
O	6.766997	-11.219995	11.995994
H	6.006997	-11.242995	11.351995
H	6.913997	-12.141994	12.265994
O	6.084997	-8.355996	14.988993
H	5.384997	-8.531996	15.635993
H	6.931997	-8.479996	15.463993
C	9.505996	-4.469998	11.739994
28			
del COeq2			
C	8.339996	-5.048998	10.900995
H	8.646996	-5.094998	9.852995
H	7.472996	-4.381998	10.983995
C	8.021996	-6.449997	11.330995
N	8.665996	-7.507996	10.711995
H	9.251996	-7.415997	9.879995
C	8.315996	-8.651996	11.325995
H	8.712996	-9.609995	11.038995
N	7.452996	-8.411996	12.306994
C	7.264997	-7.034997	12.319994
H	6.613997	-6.567997	13.041994
C	5.901997	-8.572996	14.607993
C	3.090999	-12.242994	13.283994
C	5.792997	-11.152995	14.551993
O	5.482997	-7.701996	15.245993
O	2.477999	-11.284995	13.377994
O	5.308997	-11.972994	15.216993
Mn	6.525997	-9.853995	13.505994
O	8.485996	-10.165995	14.288993
H	9.099996	-9.405996	14.234993
H	8.613996	-10.559995	15.185993
O	7.231997	-11.327995	12.126994

H	5.861997	-11.256995	11.558995
H	7.354997	-11.521995	12.038994
O	5.923997	-11.097995	15.131993
H	6.632997	-11.285995	15.771993
H	5.727997	-11.926994	14.658993
C	9.510996	-4.463998	11.739994

28
del Imi

C	8.364996	-5.100998	10.917995
H	8.658996	-5.132998	9.866995
H	7.463996	-4.486998	11.018995
C	8.163996	-6.503997	11.409995
N	8.755996	-7.563996	10.745995
H	9.206996	-7.485996	9.828995
C	8.695996	-8.655996	11.535995
H	9.084996	-9.626995	11.267995
N	8.092996	-8.355996	12.676994
C	7.740996	-7.025997	12.608994
H	7.195997	-6.535997	13.404994
C	5.068998	-8.675996	14.776993
C	5.387997	-9.227996	12.282994
C	3.584998	-10.612995	13.505994
O	4.983998	-7.663996	15.324993
O	5.378997	-8.643996	11.289995
O	2.543999	-11.007995	13.213994
Mn	5.334997	-10.203995	13.816993
O	5.318997	-11.371995	15.577993
H	5.838997	-12.184994	15.491993
H	5.752997	-10.830995	16.288992
O	5.836997	-11.912994	12.694994
H	5.503997	-11.769994	11.764994
H	6.807997	-11.833994	12.655994
O	7.393997	-10.330995	14.072993
H	7.856996	-10.491995	14.916993
H	7.792996	-9.477996	13.619994
C	9.505996	-4.463998	11.735994

29
delCOax delCOeq2

C	8.332996	-5.038998	10.895995
H	8.637996	-5.080998	9.848995
H	7.471996	-4.370998	10.983995
C	7.985996	-6.435997	11.318995
N	8.579996	-7.506996	10.678995
H	9.151996	-7.420997	9.839995
C	8.224996	-8.640996	11.319995
H	8.561996	-9.619995	11.034995
N	7.417997	-8.370996	12.336994
C	7.256997	-6.993997	12.339994
H	6.640997	-6.509997	13.077994
C	5.930997	-8.513996	14.686993
C	4.135998	-12.653994	13.310994
O	5.384997	-7.706996	15.341993
O	3.135999	-12.101994	13.301994
Mn	6.646997	-9.726995	13.626994
O	8.623996	-10.035995	14.379993
H	9.247996	-9.289996	14.277993
H	7.301997	-11.028995	11.191995
H	8.131996	-11.593995	12.402994
O	4.899998	-9.712995	12.141994
H	4.086998	-9.838995	12.652994
H	4.889998	-10.448995	11.435995
C	9.506996	-4.463998	11.738994

29
delCOax delCOeq1 (3)

C	8.335996	-5.054998	10.901995
H	8.663996	-5.138998	9.864995
H	7.491996	-4.357998	10.942995
C	7.931996	-6.425997	11.373995
N	8.497996	-7.550996	10.801995
H	9.117996	-7.522996	9.987995
C	8.040996	-8.645996	11.454995
H	8.310996	-9.652995	11.186995
N	7.192997	-8.299996	12.418994
C	7.121997	-6.916997	12.373994
H	6.487997	-6.377997	13.056994
C	5.643997	-10.894995	17.688992
C	4.507998	-9.243996	12.984994
O	5.347997	-10.541995	18.722991
O	3.402998	-9.048996	12.621994
Mn	6.089997	-9.641995	13.598994
O	8.063996	-9.981995	14.581993
H	8.820996	-9.535996	14.167993
H	8.433996	-10.593995	15.263993
O	6.361997	-11.258995	12.254994
H	5.694997	-11.257995	11.493995
H	7.226997	-11.453995	11.857994
O	5.341997	-11.301995	14.732993
H	5.701997	-12.041994	14.208993
H	5.705997	-11.365995	15.633993
O	5.903997	-8.628996	15.456993
H	5.530997	-7.740996	15.555993
H	6.796997	-8.616996	15.850993
C	9.506996	-4.467998	11.737994

29
delCOeq1 delImi

C	8.360996	-5.018998	10.867995
H	8.705996	-5.096998	9.838995
H	7.526996	-4.313998	10.907995
C	7.956996	-6.380997	11.331995
N	8.435996	-7.516996	10.697995
H	9.012996	-7.497996	9.851995
C	8.067996	-8.599996	11.413995
H	8.289996	-9.621995	11.159995
N	7.368997	-8.203996	12.468994
C	7.283997	-6.833997	12.434994
H	6.772997	-6.289997	13.207994
C	4.241998	-9.383996	13.412994
C	3.941998	-11.754994	13.816993
O	3.512998	-8.616996	12.924994
O	3.029999	-12.391994	13.476994
Mn	5.284998	-10.625995	14.145993
O	6.700997	-12.015994	14.915993
H	7.383997	-11.652995	15.514993

H	8.850996	-10.462995	15.239993
O	7.266997	-11.420995	12.403994
H	6.994997	-11.405995	11.470995
H	8.230996	-11.577995	12.406994
O	6.095997	-11.388995	14.936993
H	6.484997	-12.192994	14.551993
H	6.525997	-11.269995	15.802993
O	4.899998	-9.819995	12.335994
H	4.102998	-10.011995	12.848994
H	4.886998	-10.454995	11.560995
C	9.502996	-4.463998	11.735994

32

delCOax delImi (5)

C	8.349996	-5.028998	10.878995
H	8.693996	-5.105998	9.847995
H	7.510996	-4.326998	10.913995
C	7.927996	-6.399997	11.328995
N	8.481996	-7.533996	10.750995
H	9.080996	-7.510996	9.922995
C	7.946996	-8.623996	11.356995
H	8.194996	-9.637995	11.097995
N	7.088997	-8.257996	12.301994
C	7.068997	-6.874997	12.287994
H	6.451997	-6.327997	12.977994
C	5.799997	-8.122996	14.813993
C	4.496998	-9.261996	13.003994
O	5.486997	-7.271997	15.538993
O	3.437998	-9.197996	12.523994
Mn	6.130997	-9.465996	13.679994
O	8.105996	-10.090995	14.220993
H	8.872996	-9.496996	14.021993
H	8.335996	-10.517995	15.072993
O	6.276997	-11.203995	12.437994
H	5.721997	-11.240995	11.605995
H	7.171997	-11.508995	12.219994
O	5.550997	-10.862995	15.181993
H	5.929997	-11.734994	14.985993
H	5.893997	-10.595995	16.077992
O	10.438995	-8.725996	13.555994
H	10.829995	-9.545996	13.155994
H	10.222995	-8.179996	12.780994
O	6.568997	-10.056995	17.508992
H	6.703997	-9.208996	18.001992
H	7.402997	-10.551995	17.649992
C	9.507996	-4.465998	11.734994

30

delCOax delCOeq1 delImi(4)

C	8.345996	-5.055998	10.901995
H	8.658996	-5.112998	9.859995
H	7.487996	-4.381998	10.974995
C	8.001996	-6.442997	11.361995
N	8.598996	-7.537996	10.761995
H	9.169996	-7.482996	9.913995
C	8.271996	-8.646996	11.465995
H	8.618996	-9.636995	11.212995
H	6.373997	-12.820994	15.350993
O	6.248997	-11.039995	12.332994
H	5.641997	-11.153995	11.529995
H	6.747997	-11.869994	12.415994
O	4.848998	-10.068995	16.161992
H	5.536997	-9.361996	16.102992
H	3.985998	-9.620995	16.172992
O	6.768997	-9.299996	14.596993
H	7.609996	-9.678995	14.907993
H	7.058997	-8.804996	13.465994
C	9.514996	-4.458998	11.735994

30

delCOeq1 delCOeq2 delCOax

C	8.324996	-5.074998	10.904995
H	8.634996	-5.112998	9.855995
H	7.462996	-4.406998	10.983995
C	7.981996	-6.480997	11.328995
N	8.631996	-7.542996	10.719995
H	9.221996	-7.449996	9.893995
C	8.237996	-8.688996	11.319995
H	8.606996	-9.662995	11.032995
N	7.357997	-8.445996	12.286994
C	7.187997	-7.065997	12.294994
H	6.510997	-6.606997	12.998994
C	4.205998	-12.174994	13.925993
O	3.345998	-12.191994	13.157994
Mn	6.576997	-9.801995	13.612994
O	8.425996	-9.483996	14.773993
H	9.186996	-9.111996	14.288993
H	8.793996	-10.182995	15.362993
O	7.207997	-11.606995	12.549994
H	6.721997	-11.664995	11.710994
H	8.136996	-11.807994	12.332994
O	4.825998	-9.733995	12.230994
H	4.017998	-9.995995	12.693994
H	4.867998	-10.388995	11.464995
O	5.793997	-8.247996	14.916993
H	5.301998	-8.788996	15.563993
H	6.630997	-8.064996	15.385993
O	6.157997	-10.935995	15.497993
H	5.745997	-11.785994	15.266993
H	6.954997	-11.132995	16.020992
C	9.501996	-4.470998	11.738994

33

delCOeq1 delCOeq2 delImi

C	8.351996	-5.063998	10.901995
H	8.662996	-5.101998	9.856995
H	7.479996	-4.408998	10.985995
C	8.034996	-6.461997	11.341995
N	8.632996	-7.546996	10.726995
H	9.201996	-7.478996	9.880995
C	8.286996	-8.665996	11.389995
H	8.625996	-9.653995	11.118995

N	7.484996	-8.332996	12.486994
C	7.305997	-6.963997	12.425994
H	6.698997	-6.441997	13.147994
C	4.035998	-9.038996	13.488994
O	3.336998	-8.296996	12.894994
Mn	4.768998	-10.378995	14.315993
O	5.338997	-12.326994	15.113993
H	5.621997	-12.622994	14.225993
H	6.167997	-12.291994	15.619993
O	5.601997	-11.373995	12.645994
H	5.210998	-11.333995	11.707994
H	6.458997	-10.916995	12.563994
O	2.854999	-11.362995	14.356993
H	2.909999	-11.773994	15.240993
H	2.177999	-10.660995	14.434993
O	4.395998	-9.767995	16.331992
H	5.298998	-9.692995	16.747992
H	4.070998	-8.852996	16.300992
O	6.745997	-9.877995	14.505993
H	7.034997	-9.594995	15.397993
H	7.077997	-9.210996	13.804993
C	9.506996	-4.464998	11.735994

31
Mn wat6

C	8.346996	-5.079998	10.906995
H	8.655996	-5.135998	9.861995
H	7.475996	-4.416998	10.975995
C	8.039996	-6.475997	11.380995
N	8.564996	-7.565996	10.707995
H	9.084996	-7.497996	9.832995
C	8.315996	-8.675996	11.440995
H	8.626996	-9.666995	11.149995
N	7.649996	-8.374996	12.544994
C	7.463996	-7.006997	12.513994
H	6.932997	-6.483997	13.295994
O	3.079999	-11.525995	14.099993
H	3.733998	-12.282994	14.243993
H	2.952999	-11.128995	14.982993
Mn	5.365997	-11.087995	14.088993
O	5.787997	-12.244994	15.888993
H	6.346997	-11.733994	16.505992
H	6.274997	-13.070994	15.719993
O	6.118997	-12.444994	12.599994
H	5.831997	-12.214994	11.691994
H	7.028997	-12.097994	12.673994
O	4.512998	-9.962995	12.426994
H	3.656998	-10.339995	12.724994
H	4.703998	-10.444995	11.572995
O	4.835998	-9.628995	15.555993
H	5.567997	-9.594995	16.231992
H	4.864998	-8.764996	15.118993
O	7.429997	-10.641995	13.973993
H	7.514996	-9.713995	13.574994
H	8.082996	-10.727995	14.689993
C	9.507996	-4.465998	11.735994

N	7.485996	-8.376996	12.411994
C	7.320997	-7.000997	12.384994
H	6.709997	-6.489997	13.109994
C	3.572998	-11.732994	13.699994
O	2.480999	-12.078994	13.431994
Mn	5.217998	-11.181995	13.966993
O	5.617997	-12.477994	15.619993
H	5.811997	-11.955994	16.417992
H	6.293997	-13.179994	15.568993
O	6.207997	-12.481994	12.611994
H	5.915997	-12.367994	11.682994
H	7.110997	-12.115994	12.656994
O	5.024998	-9.822995	12.320994
H	4.909998	-10.402995	11.514995
H	5.859997	-9.320996	12.186994
O	4.837998	-9.830995	15.547993
H	5.640997	-9.493996	16.016992
H	4.252998	-9.081996	15.370993
O	7.088997	-9.334996	17.025992
H	7.723996	-10.063995	17.182992
H	7.030997	-8.844996	17.889992
O	7.320997	-10.574995	14.073993
H	7.907996	-10.628995	14.845993
H	7.443996	-9.681995	13.659994
C	9.510996	-4.464998	11.738994

Supplementary Table 10: Atomic coordinates of the QM region in the intermediate states provided in the XYZ format and in Å units. All the results are optimized at the B3LYP//DZVP level of theory with the extended QM region including Asp87 in the QM/MM method used for the UV-vis absorption spectra.

35
Mn CO3 Wat3 Im Asp87 (1)

C	8.346	-5.063	10.903
H	8.668	-5.151	9.861
H	7.499	-4.370	10.941
C	7.951	-6.441	11.374
N	8.489	-7.564	10.765
H	9.102	-7.532	9.946
C	8.024	-8.664	11.395
H	8.267	-9.669	11.108
N	7.205	-8.327	12.386
C	7.155	-6.938	12.380
H	6.556	-6.399	13.097
C	3.031	-13.079	9.886
H	2.931	-13.655	8.962
H	2.736	-13.729	10.717
C	4.520	-12.693	10.090
O	4.805	-11.479	10.358
O	5.367	-13.622	9.987
C	5.799	-8.391	14.862
C	4.585	-9.471	12.878
C	5.495	-10.978	14.808
O	5.478	-7.520	15.548
O	3.556	-9.340	12.362
O	5.055	-11.792	15.482
Mn	6.193	-9.704	13.675
O	8.173	-10.168	14.293
H	8.824	-9.459	14.142
H	8.384	-10.561	15.169
O	6.614	-11.250	12.305
H	6.082	-11.366	11.461
H	7.515	-11.598	12.209
O	6.512	-9.841	17.444
H	6.732	-9.117	18.083
H	7.243	-10.479	17.545
H_L	9.169	-4.643	11.496
H_L	2.331	-12.227	9.856

36
Mn CO2 Wat4 Im Asp87 (2)

C	8.346	-5.041	10.884
H	8.683	-5.118	9.848
H	7.503	-4.347	10.929
C	7.945	-6.417	11.336
N	8.479	-7.547	10.736
H	9.099	-7.518	9.925
C	8.002	-8.639	11.375
H	8.241	-9.650	11.101
N	7.179	-8.285	12.357
C	7.139	-6.897	12.337
H	6.540	-6.351	13.046
C	3.051	-13.051	9.901
H	2.985	-13.635	8.977
H	2.754	-13.700	10.731
C	4.533	-12.641	10.145

34
delCOax delCOeq1 Asp87 (3)

C	8.326	-5.028	10.897
H	8.650	-5.099	9.858
H	7.485	-4.327	10.952
C	7.920	-6.410	11.342
N	8.494	-7.512	10.729
H	9.109	-7.461	9.914
C	8.009	-8.628	11.315
H	8.290	-9.624	11.028
N	7.142	-8.317	12.270
C	7.082	-6.935	12.297
H	6.453	-6.432	13.009
C	3.007	-13.101	9.865
H	2.896	-13.677	8.942
H	2.704	-13.758	10.688
C	4.514	-12.770	10.065
O	4.862	-11.573	10.300
O	5.305	-13.749	9.990
C	4.555	-9.456	12.781
O	3.486	-9.377	12.285
Mn	6.153	-9.650	13.480
O	8.216	-10.040	14.232
H	8.912	-9.382	14.040
H	8.549	-10.563	14.985
O	6.554	-11.417	12.392
H	6.025	-11.485	11.537
H	7.492	-11.525	12.174
O	5.595	-11.042	15.046
H	5.909	-11.903	14.723
H	6.107	-10.837	15.853
O	5.907	-8.185	15.052
H	4.960	-8.234	15.250
H	6.347	-8.571	15.853
H_L	9.157	-4.625	11.492
H_L	2.321	-12.237	9.841

37
delCOax delCOeq1 delImi Asp87 (4)

C	8.336	-5.054	10.907
H	8.647	-5.124	9.861
H	7.478	-4.377	10.969
C	7.990	-6.438	11.382
N	8.526	-7.547	10.752
H	9.066	-7.504	9.886
C	8.209	-8.646	11.475
H	8.518	-9.643	11.211
N	7.486	-8.313	12.535
C	7.338	-6.941	12.484
H	6.780	-6.405	13.235
C	2.986	-13.115	9.853
H	2.864	-13.686	8.929
H	2.686	-13.774	10.677
C	4.487	-12.779	10.030
O	4.816	-11.562	10.225

O 4.788 -11.456 10.537 O 5.410 -13.531 9.955 C 5.781 -8.168 14.792 C 4.572 -9.299 12.967 O 5.433 -7.305 15.495 O 3.496 -9.151 12.550 Mn 6.177 -9.516 13.699 O 8.184 -10.040 14.386 H 8.876 -9.382 14.197 H 8.441 -10.479 15.230 O 6.519 -11.239 12.564 H 5.982 -11.357 11.717 H 7.453 -11.431 12.375 O 5.509 -10.929 15.126 H 6.025 -11.743 15.025 H 5.645 -10.583 16.047 O 5.553 -9.587 17.524 H 5.027 -8.798 17.311 H 6.309 -9.212 18.028 H_L 9.166 -4.630 11.487 H_L 2.336 -12.215 9.856	O 5.293 -13.743 9.982 C 4.209 -9.119 13.443 O 3.631 -8.264 12.870 Mn 4.833 -10.487 14.312 O 5.328 -12.388 15.268 H 5.424 -12.831 14.398 H 6.238 -12.372 15.615 O 5.581 -11.661 12.727 H 5.286 -11.520 11.775 H 6.527 -11.443 12.730 O 2.871 -11.376 14.479 H 2.919 -11.613 15.424 H 2.229 -10.640 14.435 O 4.464 -9.768 16.299 H 5.367 -9.718 16.725 H 4.188 -8.840 16.228 O 6.836 -10.034 14.437 H 7.138 -9.718 15.309 H 7.093 -9.321 13.743 H_L 9.160 -4.630 11.493 H_L 2.313 -12.244 9.835

Supplementary References

1 Adams, P. D. *et al.* PHENIX: a comprehensive Python-based system for macromolecular structure solution. *Acta Crystallographica Section D* **66**, 213-221 (2010). https://doi.org:doi:10.1107/S0907444909052925

2 McCoy, A. J. *et al.* Phaser crystallographic software. *J. Appl. Crystallogr.* **40**, 658-674 (2007). https://doi.org:doi:10.1107/S0021889807021206

3 Vaney, M. C., Maignan, S., Ries-Kautt, M. & Ducruix, A. High-Resolution Structure (1.33 A) of a HEW Lysozyme Tetragonal Crystal Grown in the APCF Apparatus. Data and Structural Comparison with a Crystal Grown under Microgravity from SpaceHab-01 Mission. *Acta Crystallographica Section D* **52**, 505-517 (1996). https://doi.org:doi:10.1107/S090744499501674X

4 Razavet, M. *et al.* Tricarbonylmanganese(i)–lysozyme complex: a structurally characterized organometallic protein. *Chem. Commun.*, 2805-2807 (2007). https://doi.org:10.1039/B703887A

5 Nango, E. *et al.* A three-dimensional movie of structural changes in bacteriorhodopsin. *Science* **354**, 1552-1557 (2016). https://doi.org:10.1126/science.aah3497

6 Chen, V. B. *et al.* MolProbity: all-atom structure validation for macromolecular crystallography. *Acta Crystallographica Section D* **66**, 12-21 (2010). https://doi.org:doi:10.1107/S0907444909042073